ON THE VERGE OF BIOORGANIC AND INORGANIC CHEMISTRY: METALLACARBORANES IN NANOMEDICINE

Adnana Alina Zaulet

TESI DOCTORAL

Programa de Doctorat en Química

Director: Prof. Clara Viñas i Teixidor

Tutor: Josefina Pons Picart

Departament de Química

Facultat de Ciències

2015

CONCLUSIONS

CONCLUSIONS

We synthesized and characterized several sets of anionic methylated and halogenated metallabis(dicarbollide) clusters and studied the electrochemical properties of all complexes. The electronic effect of the substituent (Me or I) bonded *exo*-cluster to boron vertexes influence on the $E_{1/2}$ of the metal based electrochemical response (Co^{III}/Co^{II} or Fe^{III}/Fe^{II}). The π-back donation by I lone pairs produces an opposite and larger effect than alkyl substituent groups. The $E_{1/2}$ substituent site dependence is also clear so all the results are related to the B-I vertex distance to the Fe or Co metal center. By the tuning of the scaffold $[M(C_2B_9H_{11})_2]^-$ it is possible to modify the $E_{1/2}$ in a controlled manner.

The $E_{1/2}$ of the couple $[I_8\text{-}\mathbf{3}]^{-/2-}$ (-0.68 V *vs* $Fc^{+/0}$) (cobalt centered) and $[Cl_6\text{-}\mathbf{4}]^{-/2-}$ (+0.00 V *vs* $Fc^{+/0}$) (iron centered) allows both the oxidized and reduced forms to stand in air for several hours and days. Based on these features, we selected the couple $[Cl_6\text{-}\mathbf{4}]^{-/2-}$ to be tested as electroactive electrolytes in the DSSC devices. It was compared with the commercially available Dyesol's EL-HSE, which is an liquid electrolyte based on the I^-/I_3^- redox couple. The results showed that the hexachlorinated ferrabis(dicarbollide) electrolytes have very low performances with respect to the common iodine based electrolyte. Maybe it is due to their steric hindrance that they suffer from ionic motility between the two cell electrodes.

We have studied the electrochromic behavior of the $[MV][Cl_6\text{-}\mathbf{4}]_2$ through electrolysis experiments. Four different colors (orange, navy blue, pink and green) have been observed for the same compound corresponding to different electronic transitions taking place on different site of the molecule.

Another subject was the synthesys, isolation and characterization of different salts of the parent cobaltabis(dicarbollide) and some of its derivatives. $^{11}B\{^1H\}$ and $^1H\{^{11}B\}$-NMR studies in D_2O of H[**3**], Li[**3**], Na[**3**], K[**3**], H[I-**3**], Na[I-**3**], H[I_2-**3**] and Na[I_2-**3**] at different concentrations were carried out. $^{11}B\{^1H\}$-NMR spectra of Li[**3**], Na[**3**] and K[**3**] shows wider resonances at concentrations higher than 10 mM indicating the presence of micelles, as reported by H[**3**] that is taken as a reference. $^1H\{^{11}B\}$-NMR spectra of H[**3**], Li[**3**], Na[**3**] and K[**3**] indicate that the resonance of the C_c-H remains invariant in the concentration range 2.5 - 10 mM in which, the vesicles are formed. However, when the concentration increases till 20 mM at which concentration the

micelles are formed, the C_c-H resonance is shifted upfield for all salts. In the case of the monoiodinated species [I-**3**]$^-$ it is concluded that aggregates are produced either from its H^+ or Na^+ salt at concentration higher that 15 mM. In the case of [I_2-**3**]$^-$, by using different methods, several ordered and disordered phases were identified over a large range of temperature and concentration. In the diluted regime, H[I_2-**3**] was found to behave similarly as H[**3**] by forming vesicles with a radius of gyration of around 98.3 nm and at high concentrations forms lyotropic lamellar phases structures. It was concluded that the formation of intermolecular hydrogen bonds, such as –C_c-$H^{\delta+}$…$^{\delta-}$H-B-, is the driving force in the lamella formation.

The behavior of the sodium salt of the anion [**4**]$^-$ in aqueous solution as a function of the concentration was also studied. $^{11}B\{^1H\}$-NMR spectra remain unaltered from 5 to 20 mM but, they are slightly shifted to a higher field at concentrations higher than 30 mM. If we compare the effect of the concentration in the $^1H\{^{11}B\}$-NMR of Na[**4**] and Na[**3**] species, we observe that the difference is 9.16 ppm for Na[**4**] and 0.13 ppm for Na[**3**] when concentration increases from 5 mM to 60 Mm in both cases.

The cleavage of the dioxane ring of the zwitterionic derivative of cobaltabis(dicarbollide), **5**, and ferrabis(dicarbollide) **6**, was achieved by employing biomolecules such as vitamins (B_3 vitamin), fatty acids (palmitic acid) and sugars among others. The resulting species were characterized by IR, MALDI-TOF and ^1H, ^{11}B and ^{13}C NMR techiniques.

The radio imaging studies *"in vivo"* have been performed after the synthesis of new bi-functional (iodine and polyethylene glycol, PEG) metallabis(dicarbollide) derivatives that incorporate simultaneously two markedly different reactive sites: a PEG branch and a suitable iodinated moiety for subsequent incorporation of the radioisotope. We developed a strategy to covalently label this compounds with either ^{125}I (gamma emitter) or ^{124}I (positron emitter) via palladium catalyzed isotopic exchange. Biodistribution studies using dissection and gamma counting were performed in rodents with the compounds Na[^{125}I-**7**] / Na[^{124}I-**7**] and Na[^{125}I-**3**]/Na[^{124}I-**3**]. Very similar patterns were obtained for both compounds: high accumulation in the liver throughout the duration of the study, increasing uptake in the lungs and moderate blood clearance. Uptake in the kidneys and the spleen was also significant and lower accumulation was detected in other organs.

Biodistribution PET studies with the labeled compounds (K[^{124}I-**9**], H[^{124}I-**14**] and Na[^{124}I-**3**]) were carried out in subcutaneous PANC-1 and A547 xenograft mouse

models. [^{18}F]FDG was used as reference. Unfortunately, comparing with the [^{18}F]FDG, the accumulation in the tumour for the compounds K[^{124}I-**9**], H[^{124}I-**14**] and Na[^{124}I-**3**], was relatively low.

ADDENDUM

Boron Cluster Lamellar Phases

DOI: 10.1002/anie.201307357

Lyotropic Lamellar Phase Formed from Monolayered θ-Shaped Carborane-Cage Amphiphiles**

Damien Brusselle, Pierre Bauduin, Luc Girard, Adnana Zaulet, Clara Viñas, Francesc Teixidor, Isabelle Ly, and Olivier Diat*

Lyotropic lamellar phases occur naturally and are a key architectural feature for life to develop as they enable the formation of closed-cell topologies.[1] But in addition to closed-cell topologies, enabling life means that the same solvent must be on both sides of the cell membrane, hence at least a double-layered membrane structure is necessary. For this a lamellar phase must be enabled. Herein we show that the formation of lamellar phases is not exclusive to alkyl-chain-based surfactants with a well-defined amphiphilic structure but that it can also be obtained with metallacarborane clusters, described previously as θ-shaped amphiphiles.[2] Similarly to phospholipid cell membranes the lamellae formed can exist both in the liquid and in the solid states depending on temperature. The determination of the 2D molecular arrangement in the lamella demonstrated that the formation of intermolecular dihydrogen bonds, such as -C-$H^{\delta+}$...$^{\delta-}$H-B-, is the driving force in the lamella self-assembly process. Compared to the common bilayer structure that originates from the hydrophobic effect,[3] θ-shaped amphiphiles form lamellae with a peculiar monomolecular structure reminiscent of lamellar sheets observed in inorganic layered systems.[4] Nano-scale ordering of planar organic–inorganic hybrid sheets is controlled by temperature and concentration through a self-assembly process.

The lyotropic lamellar phase, characterized by an elementary smectic liquid-crystal symmetry, is by far the most common surfactant mesophase.[5] A vast literature can be found on the topic as it shows practical applications in many different fields, such as in detergents, pharmaceutics,[6] food,[7] or materials synthesis as templates.[8] Its mesostructure consists of parallel stacks of bilayers, the structural unit of biological membranes, separated by water layers. To distinguish between molten and frozen states of the surfactant alkyl chains, lamellar phases are referred to as L_α and L_β (or "gel phase").[9] Therefore the surfactant has a liquid-like mobility in L_α whereas chain motions are highly restricted in L_β, mostly limited to rotation about the chain axis as is the case in rotator phases formed in long-chain alkanes. Surfactants in the bilayers have mostly an *all-trans* alkyl-chain conformation with possible chain inter-digitation or chain tilt in the case of L_β. Lyotropic lamellar phases have only been observed with molecules that have a well-defined amphiphilic character.

Herein, we show that metallabis(dicarbollide derivatives),[10] large anions with amphiphilic properties, form lyotropic lamellar phases at high concentrations in water. In previous studies, the surfactant-like properties of cobaltabis(-dicarbollide) anion ($[COSAN]^-$ with H^+ as the counterion) were highlighted.[2,11] Even though the central region of $[COSAN]^-$ around the cobalt atom is more polar (and locally charged) than its two extremities,[12] H[COSAN] (Figure 1) does not show a classical amphiphilic structure and was therefore named θ-shaped amphiphile in reference to its molecular shape. H[COSAN] self-assembles in water by forming isotropic phases: vesicles of monomolecular thickness in diluted regime that turn into small micelles by increasing concentration.

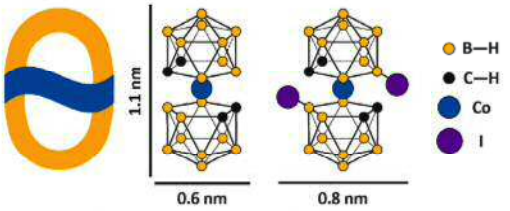

Figure 1. Chemical structure of the amphiphilic ion, $[COSAN]^-$ (left), and its diiodinated derivative, $[I_2COSAN]^-$ (right) whose shape is compared to the Greek letter θ (far left).

We focus herein on the diiodo-COSAN ($[I_2COSAN]^-$ with H^+ as counterion, Figure 1) by determining the temperature–concentration (T/ϕ) phase diagram[13] of the binary system with water that shows the occurrence of anisotropic birefringent phases (Figure 2). By combining visual observa-

[*] D. Brusselle, Dr. P. Bauduin, Dr. L. Girard, Dr. O. Diat
ICSM, UMR 5257 (CEA, CNRS, UM2, ENSCM)
CEA Marcoule
BP 17171, 30207 Bagnols-sur-Cèze (France)
E-mail: Pierre.Bauduin@cea.fr
A. Zaulet, Prof. C. Viñas, Prof. F. Teixidor
ICMAB (CSIC)
Campus de la UAB 08193 Bellaterra (Spain)
I. Ly
Centre de Recherche Paul Pascal (CRPP)
CNRS 115 av. Schweitzer F-33600 Pessac (France)

[**] This work was supported by the Presidency and the scientific committee of the University of Montpellier II. We would like to thank O. Mondain-Monval, J. Cambedouzou, S. Prevost, J.C. Gabriel, and Th. Zemb for fruitful discussions on, respectively, the interpretation of the TEM pictures, on the 2D-crystallographic structure determination, on small-angle scattering data (and production of the 3D graphical artwork) and on the properties of rigid bilayers. Bruno Corso was very helpful for technical support with the SWAXS apparatus. This research has been financed by MEC (CTQ 2010-16237) and Generalitat de Catalunya (2009/SGR/00279). A.Z. is enrolled in the Ph.D. program of the UAB.

Supporting information for this article is available on the WWW under http://dx.doi.org/10.1002/anie.201307357.

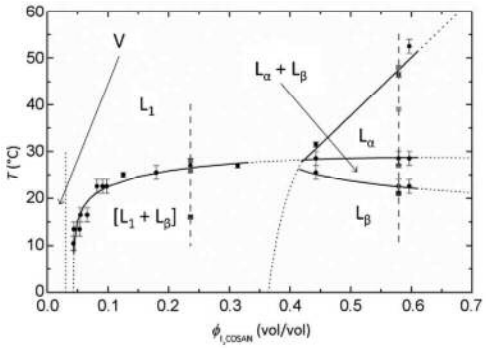

Figure 2. Binary phase diagram of H[I_2COSAN] in water showing the existence of lamellar lyotropic phases, L_α and L_β, isotropic micellar (L_1) and vesicular (V) phase. [$L_1 + L_\beta$] refers to a "gel" phase being a microscopic demixion of L_1 and L_β. Round data points correspond to experimental transition phase limits. The vertical dashed lines correspond to the samples at the two concentrations considered in Figure 4 concerning the SAXS study at different temperatures (squares).

tions, dynamic and static light scattering (DLS/SLS), small- and wide-angle X-ray scattering (SWAXS), $^{11}B\{^1H\}$ NMR spectroscopy, polarized optical light microscopy (POM) and freeze-fracture electron microscopy (FF-TEM), several ordered and disordered phases were identified over a large range of temperature and concentration.

In the diluted regime, H[I_2COSAN] is found to behave similarly as H[COSAN] by forming vesicles with a radius of gyration of around 98.3 nm as determined by DLS/SLS (see Supporting information, Figure S1). At high concentrations above 35% v/v, optical microscopy pictures show birefringence with the presence of Maltese crosses (left side in Figure 3a) that are typical of lamellar phases. Applying a soft shear stress, by sliding the microscopy slide cover slip, the system can be easily mechanically aligned over one centimeter square (right side of Figure 3a). At temperatures below

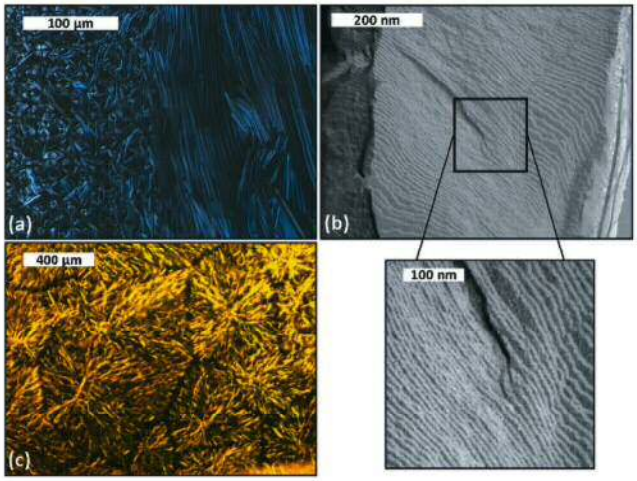

Figure 3. a) Polarized optical microscope images of the "gel" phase [$L_1 + L_\beta$], b) freeze-fracture TEM picture of the pure L_β phase showing the lamellar arrangement with an apparent inter-lamellar distance of roughly 5 nm confirmed by SWAXS, and c) optical microscope picture showing a spherulite texture of the "gel" phase [$L_1 + L_\beta$].

20 °C and volume fractions above 40% SWAXS spectra show in the low q-range a series of diffraction peaks with a 1:2:3:4 ... ratio which is a signature of a lamellar ordering (see the spectrum at 21 °C in Figure 4b) that confirms the microscopy observation. The occurrence of many sharp peaks in the large q-range, above 8 nm^{-1} indicates a supplementary solid-like molecular ordering typical of L_β phase. By increasing temperature above 27 °C, these Bragg peaks turn into a broad peak centered at 9.7 nm^{-1} ($d = 0.65$ nm) characteristic of the melting effect within the lamella. The H[I_2COSAN] molecules of the layers undergo here a transition from solid- to fluid-like behavior which is the characteristic of a L_β to L_α transition. This transition was confirmed by $^{11}B\{^1H\}$ NMR spectra of 1 M solution of H[I_2COSAN] in water as function of T °C, see Figure S2. Between 20 and 27 °C two series of Bragg peaks in the low q regime are observed (see Figure 4b at 27 °C) indicating that L_β and L_α phases coexist and that the transition is first order. The lamella thickness (δ) can be estimated from d^* values, the periodicity of the lamellar structure, and the [I_2COSAN]$^-$ volume fraction, ϕ, with $d^* = \delta/\phi$. δ lies between 1.1 and 1.4 nm which is in the order of the molecular length (ca. 1.1 nm for the molecular long axis). Therefore the lamellae are made of monomolecular layers with the H[I_2COSAN] molecules oriented orthogonally to the lamella plane. It has already been shown that H[COSAN] adopts such a molecular arrangement in the wall structure of vesicles formed in the diluted regime.[2] By increasing further the temperature, the solution becomes isotropic with no birefringence and is referred to as the micellar phase, L_1.

At intermediate concentrations, between around 4–5% (around 100 mM) and 40% v/v a stable highly viscous "gel" is observed at temperatures below 25 °C. Optical microscopy shows birefringent micrometric inhomogeneity ("hairy-like") with a large millimetric spherullitic texture (Figure 3c) which is commonly observed during crystallization of polymer melts in highly ordered lamellar regions.[14] SWAXS spectra in this concentration regime also show a series of diffraction peaks with a 1:2:3:4... ratio in the low q values and Bragg peaks in the large q domain, above 8 nm^{-1}, as in the pure L_β phase (Figure 4b). However, the SWAXS spectra differ from the one observed with the L_β at higher concentrations. A broad peak is superimposed on the scattering curves and presents a maximum intensity at q values around 1 nm^{-1}, depending on concentration. This contribution to the scattered intensity can be attributed to the presence of nano-aggregates as it was previously concluded for H[COSAN] in a similar concentration range.[2] These aggregates were described in a first approximation as small spherical micelles with an average aggregation number of approximately 12 and with a radius of around the length of the COSAN ion that is, 1.1 nm. Increasing temperature induces the melting of the gel in a pure isotropic micellar phase, L_1 (Figure 2). This transition is concomitant with the disappearance of the lamellar signature in the SWAXS spectra, leaving only the micelle signal (Figure 4a, upper curve).[2] Consequently the "gel" phase is made of a mixture of L_1 and L_β phases dispersed in micro-domains that do not phase separate macroscopically. Such local segregations of two distinct phases, lamellar and diluted phases, on a colloidal scale has been observed with

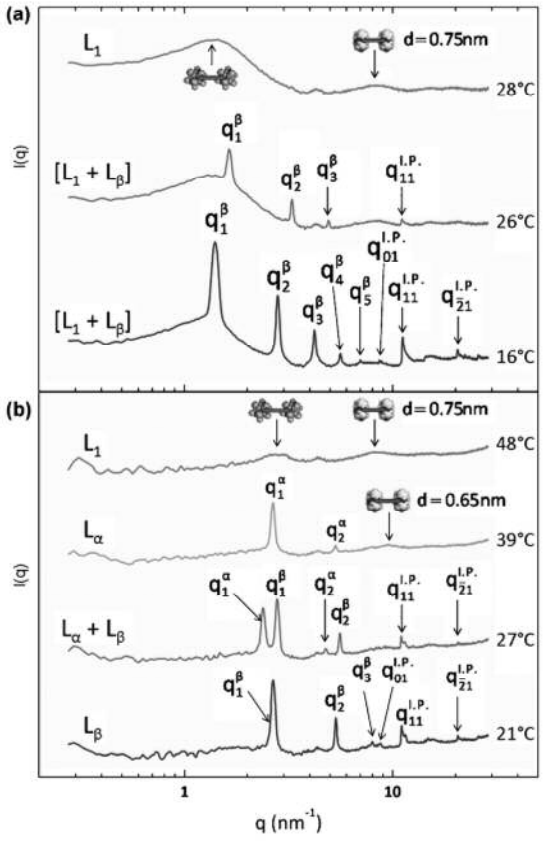

Figure 4. SWAXS spectra of H[I_2COSAN] in water at different temperatures at a) 23.5 and b) 59% v/v.

some double-chained surfactant systems[15] as well as in purely inorganic clay systems forming the so-called tactoids.[16] For surfactant systems the notation $[L_1+L_\beta]$ or $[L_\beta]$ is commonly used to refer to such $L_\beta+L_1$ dispersions.

The inter-lamellar distance (d^*) in the L_β micro-domains of the $[L_1+L_\beta]$ phase can also be calculated from the position of the first order peak in SWAXS spectra such as $d^*=2\pi/q$. Dilution, as well as a decrease in temperature, leads to exfoliation (or swelling) of the lamellae whose periodicity range from approximately 2 up to around 7 nm that corresponds to the maximum swelling (Figure S3). Pictures of the lamellar arrangement in the L_β phase obtained by freeze-fracture transmission electron microscopy (FF-TEM) confirm the 1D long range ordering of the lamella as inferred from the sharpness of the peaks observed in SWAXS as well as the order of magnitude of d^* (Figure 3b). Swelling of layered systems is a general process observed for example during the dilution of lamellar phases made of surfactants, inorganic covalently bound sheets such as clays[17] or other systems made of phosphatoantimonate layers.[18]

At constant temperature in the $[L_1+L_\beta]$ region d^* continuously decreases by increasing H[I_2COSAN] concentration (Figure S3) whereas the intensity of the micelles signal, which is related to the micelle concentration, decreases (Figure S4). Therefore the compositions in the micro-phases change continuously while the concentration varies. As a consequence, the biphasic $[L_1+L_\beta]$ region does not represent the case of a macroscopic phase separation with identified tie lines. For a macroscopic phase separation between a lamellar phase and a second liquid phase the osmotic equilibrium condition, that is, $|\pi_1-\pi_2|=0$ with π_i the osmotic pressures in the two phases in equilibrium, sets the spacing observed between the lamellae.[19] In the present case the interfacial energy of contact between the two micro-phases cannot be neglected in the thermodynamic analysis leading to the master equation $|\pi_{L\beta}-\pi_{L1}|=\gamma A$ with γ and A the interfacial tension and specific surface between the micro-phases respectively. For macroscopic dispersions, the large size of the domains leads to small specific surfaces and to a negligible contribution of the interfacial energy resulting in a constant d^* value along a given tie line when concentration is varied. Consequently, the variation in d^* observed at constant temperature can be explained by considering a significant contribution of the interfacial energy between the micro-phases.[15]

To go further in the determination of the lamella molecular organization, the position of the three main Bragg peaks observed at around 8.6, 11.2, and 20.5 nm^{-1} (Figure 4) in the pure L_β and in the biphasic $[L_1+L_\beta]$ phases can be analyzed. These peaks correspond to the diffraction of crystallographic planes within the monolayer (in-plane diffraction peaks noted $q^{I.P.}$), as inferred from the saw-tooth shape of the peaks,[20] while the diffraction peaks (q^α or q^β) observed at lower q values correspond to out-of-plane diffraction. The peaks positions could be well indexed with an oblique lattice, with lattice parameters $a=b=7.4$ Å and $\theta=80.5°$, which is one of the five types of the 2D Bravais lattices. The peaks in the SAXS spectra were then indexed according to the crystallographic planes (01) or (10), (11), and ($\bar{2}$1), respectively, for the first, second, and third peak observed. We can thus propose a 2D lattice of the lamellae, as shown in Figure 5, which is in good agreement with the molecular distances with one $[I_2COSAN]^-$ ion per lattice. In this structure it was considered that $[I_2COSAN]^-$ ions present a twofold symmetry with the two iodine atoms in *trans* position, as shown in Figure 1, which represents the most stable rotamer, that is, *transoid*, as supported by the crystal structures (codes DEXPIF, IHOHAP, IHOHET, and IHOHIX) in the Cambridge Structural Database. The 2D arrangement shows that $[I_2COSAN]^-$ ions are not in close contact but are separated by a distance of 3.5 Å that may be due to the presence of intermolecular dihydrogen bonds, such as -C-$H^{\delta+}$...$^{\delta-}$H-B- or B-$H^{\delta+}$...$^{\delta-}$H-B, reducing the energy of the crystal. Such dihydrogen bonds are observed in the solid state for the [BEDT-TTF][I_2COSAN] (CSD code IHOHAP)[21] which has dihydrogen B-$H^{\delta+}$...$^{\delta-}$H–B bonds of 3.500 Å matching the value found in our case (Figure S7). According to the 2D structure, it is then likely that the self-assembly process of $[I_2COSAN]^-$ ions in monomolecular lamella relies on a network of such H-bonds while the formation of bilayers with classical surfactants is mainly driven by the hydrophobic effect. Interestingly the molecular area occupied by a $[I_2COSAN]^-$ ion in the monolayer decreases from 53.9 $Å^2$, that is, the area of the 2D crystal lattice, in the L_β phase, to 43 $Å^2$ in the L_α phase. This latter surface area was calculated as the square of the average

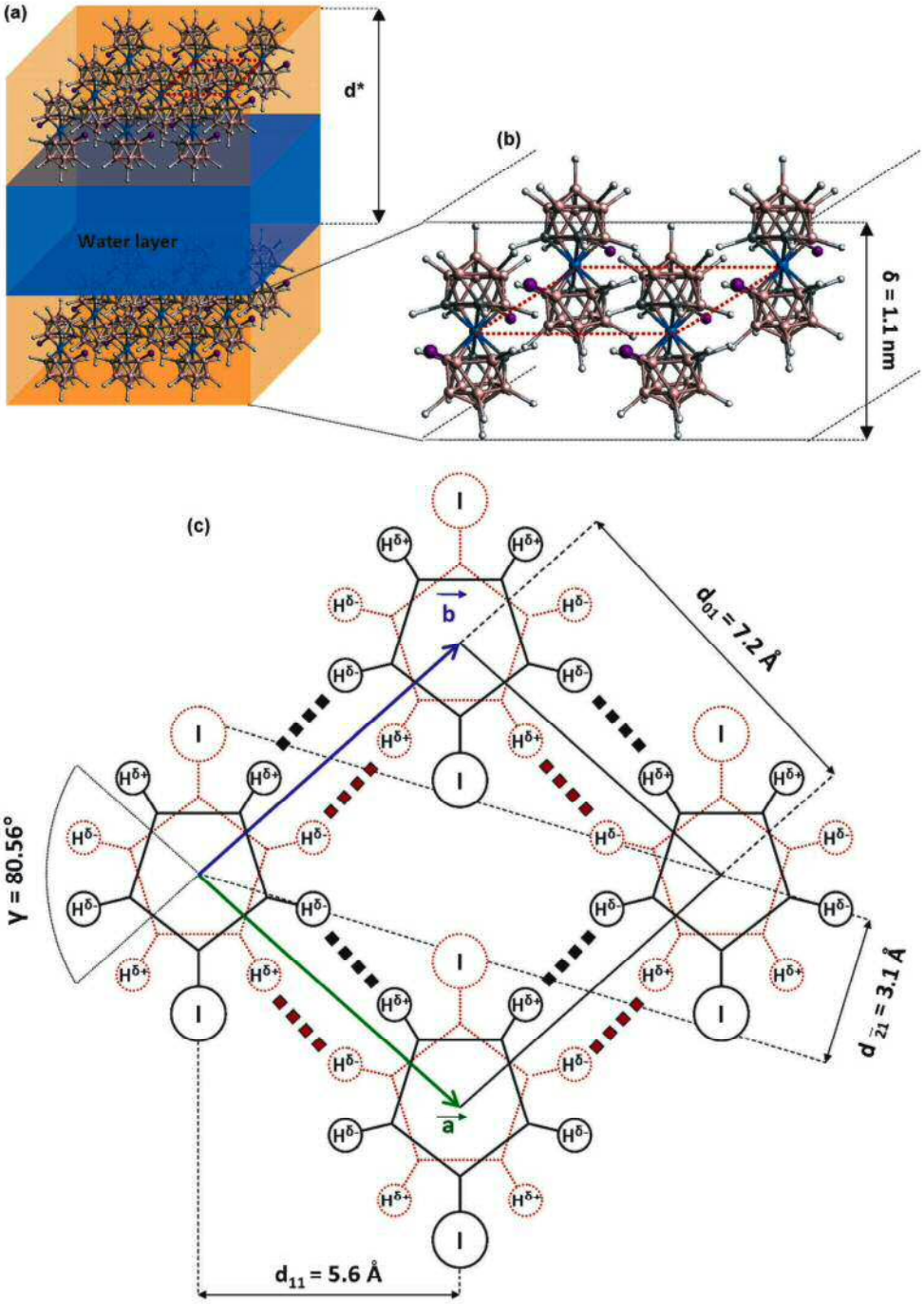

Figure 5. Molecular representation of the lamellae formed by I_2COSAN in water: a) lamellar phase showing smectic arrangements of I_2COSAN monomolecular layers and water layers, b) lateral view of the lamella and c) schematic representation crystal lattice of the 2D structure showing selected interatomic distances. Hydrogen bonds indicated by broken lines.

distance between $[I_2COSAN]^-$ molecules (6.6 Å) given by the broad peak position in the L_α phase at 9.4 nm^{-1}. Consequently the density in the film increases during the solid-to-liquid phase transition, like water does when it turns from ice into its liquid state, which is an indication for an intermolecular H-bond network being strongly involved in the structuration of the 2D I_2COSAN film. Note that the I_2COSAN density increases by about 29% $(1-(A_{L\alpha})^{3/2}/(A_{L\beta})^{3/2})$ during the L_β–L_α transition whereas the density of water increases only by 8% from ice to liquid water. This significant difference may be related to the large difference in the H-bond length between water, around 1.97 Å, and I_2COSAN. Moreover the increase in the interlamellar spacing while melting (Figure S2) may indicate that the I_2COSAN molecules also partly disorder out of plane disorder.

Further increase in the temperature leads to L_α–L_1 transition that shows a dramatic change in the aggregate curvature from plane interface to small nanometric micelles. Such a transition is ubiquitous in most surfactant binary phase diagrams.[13] During this transition the average molecular area further increases from 43 to 57.8 $Å^2$, calculated as the square of the average intermolecular distance between H[I_2COSAN] molecules (7.6 Å) a value determined from the broad peak position in the L_1 phase at 8.0 nm^{-1}. For H[COSAN] micelles the intermolecular peak position was found at higher q values, 10.8 nm^{-1} ($d = 0.56$ nm)[2] compared to 8.0 nm^{-1} ($d = 0.785$ nm) for $[I_2COSAN]^-$ the difference being explained by the presence of the two bulky iodine atoms that increases the distance between closest neighbor molecules. The increase in the molecular area from L_α to L_1 phase can be rationalized in terms of a decrease in the packing parameter, P[22] which is a geometrical parameter giving a relationship between the molecular structure and the aggregate state ($P = 1$ for plane structures, $P = 1/2$ for cylinders, and $P = 1/3$ for spheres). P is defined as $P = v/al$, with v, the molecular volume, a, the molecular area, and l, the molecular length. As v and l are constant, the temperature induced transition from L_α to L_1 phase is then controlled by the increase in a as noticed experimentally by the increase in the average distance between close neighbor molecules.

In conclusion, we have shown that the $[I_2COSAN]^-$ macro ion combines properties of purely organic surfactants and purely inorganic sheet systems, such as clays. Similarly to surfactants $H[I_2COSAN]$ self-assemble in layers that 1) form lyotropic lamellar phases in the concentrated regime, 2) that are able to bend into (closed) vesicles in the dilute regime, and that 3) show a transition from solid-like to liquid-like state on increasing temperature. On the other hand, lamellas formed by $H[I_2COSAN]$ are made of monomolecular sheets, such as clay systems, but with the sole difference that they are not covalently bound. The cohesive energy between $[I_2COSAN]^-$ ions, that leads to the lamella formation, originates presumably from intermolecular dihydrogen bonds whose formation is possible owing to the different polarity of the B–H bond vertexes in the $[I_2COSAN]^-$ cluster. Monolayers of $[I_2COSAN]^-$ are less rigid than purely inorganic covalently bound sheets so their bending is then accessible with thermal energy leading to the formation of vesicles which is not possible with clay systems. The formation of a lamellar phase seems to be a general property of metallabis(dicarbollide) systems as it could also be detected with H[COSAN] but at higher concentrations (see the SWAXS spectra Figure S6). This information on the intermolecular forces involved in the self-assembly of COSAN derivatives in water is essential for a rational design for their applications in many different fields, such as in the reprocessing of spent nuclear fuel,[23] in analytical chemistry as main component in ion-selective electrodes,[24] in solar cells design as fast redox shuttle,[25] in medicine as promising building block for drug design,[26] or in boron-neutron capture therapy.[27] The organic–inorganic hybrid lamellar phases studied could have potential applications as new liquid-crystal systems for display or memory storage if the cobalt center can be replaced with a magnetic atom, such as iron. The tunable oxidation state of the theta-shaped amphiphile metal[28] could also be used to design active nano-materials for sensing and for photonic applications.

Received: August 21, 2013

Keywords: amphiphiles · carboranes · hydrogen bonds · lamellar phases

[1] a) Y. Talmon, D. F. Evans, B. W. Ninham, *Science* **1983**, *221*, 1047–1048; b) C. R. Safinya, E. B. Sirota, R. F. Bruinsma, C. Jeppesen, R. J. Plano, L. J. Wenzel, *Science* **1993**, *261*, 588–591; c) E. W. Kaler, A. K. Murthy, B. E. Rodriguez, J. A. Zasadzinski, *Science* **1989**, *245*, 1371–1374; d) T. Zemb, M. Dubois, B. Deme, T. Gulik-Krzywicki, *Science* **1999**, *283*, 816–819; e) H. Shen, A. Eisenberg, *Angew. Chem.* **2000**, *112*, 3448–3450; *Angew. Chem. Int. Ed.* **2000**, *39*, 3310–3312; f) D. Volodkin, Y. Arntz, P. Schaaf, H. Moehwald, J. C. Voegel, V. Ball, *Soft Matter* **2008**, *4*, 122–130.

[2] P. Bauduin, S. Prevost, P. Farras, F. Teixidor, O. Diat, T. Zemb, *Angew. Chem.* **2011**, *123*, 5410–5412; *Angew. Chem. Int. Ed.* **2011**, *50*, 5298–5300.

[3] C. Tanford, *Science* **1978**, *200*, 1012–1018.

[4] Q. Wang, D. O'Hare, *Chem. Rev.* **2012**, *112*, 4124–4155.

[5] a) S. Hassan, W. Rowe, G. J. Tiddy, *Surfactant Liquid Crystals in Handbook of Applied Surface and Colloid Chemistry* (Ed.: K. Holmberg), Wiley, Chichester, **2001**, p. 465; b) S. Hyde, *Identification of Lyotropic Liquid Crystalline Mesophases in Handbook of Applied Surface and Colloid Chemistry* (Ed.: K. Holmberg), Wiley, Chichester, **2001**, pp. 299–332; c) W. Gelbart, A. Ben-Shaul, D. Roux. Micelles, *Membranes, Microemulsions, and Monolayers*, Springer, Berlin, **1994**.

[6] I. Amar-Yuli, D. Libster, A. Aserin, N. Garti, *Curr. Opin. Colloid Interface Sci.* **2009**, *14*, 21–32.

[7] a) R. Mezzenga, *Self-Assembled Food Mesophases.* Research Worlds—Focus on Food. Alimentarium Foundation Editions, **2009**; b) K. Larsson, *Curr. Opin. Colloid Interface Sci.* **2009**, *14*, 16–20.

[8] K. Na, M. Choi, W. Park, Y. Sakamoto, O. Terasaki, R. Ryoo, *J. Am. Chem. Soc.* **2010**, *132*, 4169–4177.

[9] H. Yao, I. Hatta, R. Koynova, B. Tenchov, *Biophys. J.* **1992**, *61*, 683–693.

[10] a) P. Farràs, E. J. Juárez-Pérez, M. Lepšik, R. Luque, R. Núñez, F. Teixidor, *Chem. Soc. Rev.* **2012**, *41*, 3445–3463; b) F. Teixidor, *J. Organomet. Chem.* **2009**, *694*, 1587–1587.

[11] P. Matejicek, P. Cigler, K. Prochazka, V. Kral, *Langmuir* **2006**, *22*, 575–581.

[12] P. Farras, C. Viñas, F. Teixidor, *J. Organomet. Chem.* **2013**, DOI: 10.1016/j.jorganchem.2013.03.039.

[13] R. G. Laughlin, *The aqueous phase behavior of surfactants*, Academic Press Limited, San Diego, **1994**.

[14] G. Menges, E. Haberstroh, W. Michaeli, E. Schmachtenberg, *Plastics Materials Science*, Hanser Fachbuchverlag, Leipzig, **2011**.

[15] M. Dubois, T. Zemb, *Langmuir* **1991**, *7*, 1352–1360.

[16] M. Morvan, D. Espinat, R. Vascon, J. Lambard, T. Zemb, *Langmuir* **1994**, *10*, 2566–2569.

[17] L. J. Michot, I. Bihannic, S. Maddi, S. S. Funari, C. Baravian, P. Levitz, *Proc. Natl. Acad. Sci. USA* **2006**, *103*, 16101–16104.

[18] J. C. P. Gabriel, F. Camerel, B. J. Lemaire, H. Desvaux, P. Davidson, P. Batail, *Nature* **2001**, *413*, 504–508.

[19] D. Gazeau, T. Zemb, M. Dubois, *Prog. Colloid Polym. Sci.* **1993**, *93*, 123–129.

[20] B. E. Warren, *Phys. Rev.* **1941**, *59*, 693–698.

[21] O. N. Kazheva, G. G. Alexandrov, A. V. Kravchenko, V. A. Starodub, I. A. Lobanova, I. B. Sivaev, V. I. Bregadze, L. V. Titov, L. I. Buravov, O. A. Dyachenko, *J. Organomet. Chem.* **2009**, *694*, 2336–2342.

[22] J. N. Israelachvili, D. J. Mitchell, B. W. Ninham, *J. Chem. Soc. Faraday Trans.* **1976**, *72*, 1525–1568.

[23] G. Chevrot, R. Schurhammer, G. Wipff, *J. Phys. Chem. B* **2006**, *110*, 9488–9498.

[24] A. I. Stoica, C. Viñas, F. Teixidor, *Chem. Commun.* **2009**, 4988–4990.

[25] T. C. Li, A. M. Spokoyny, C. X. She, O. K. Farha, C. A. Mirkin, T. J. Marks, J. T. Hupp, *J. Am. Chem. Soc.* **2010**, *132*, 4580–4583.

[26] a) E. Meggers, *Angew. Chem.* **2011**, *123*, 2490–2497; *Angew. Chem. Int. Ed.* **2011**, *50*, 2442–2448; b) J. Rak, B. Dejlova, H. Lampova, R. Kaplanek, P. Matejicek, P. Cigler, V. Kral, *Mol. Pharm.* **2013**, *10*, 1751–1759.

[27] E. L. Crossley, E. J. Ziolkowski, J. A. Coderre, L. M. Rendina, *Mini-Rev. Med. Chem.* **2007**, *7*, 303–313.

[28] M. F. Hawthorne, J. I. Zink, J. M. Skelton, M. J. Bayer, C. Liu, E. Livshits, R. Baer, D. Neuhauser, *Science* **2004**, *303*, 1849–1851.

ChemComm

COMMUNICATION

View Article Online
View Journal | View Issue

Cite this: *Chem. Commun.*, 2014, 50, 11415

Received 2nd July 2014,
Accepted 31st July 2014

DOI: 10.1039/c4cc05058d

www.rsc.org/chemcomm

COSAN as a molecular imaging platform: synthesis and "*in vivo*" imaging†

Kiran B. Gona,[a] Adnana Zaulet,[b] Vanessa Gómez-Vallejo,[a] Francesc Teixidor,[b] Jordi Llop*[a] and Clara Viñas*[b]

A labelling method for the covalent attachment of radioiodine to the boron-rich 8-I-cobaltabisdicarbollide (I-COSAN) and a bi-functional (iodine and PEG) COSAN derivative, [3,3′-Co(8-I-1,2-$C_2B_9H_{10}$)-(8′-$(OCH_2CH_2)_2COOC_6H_5$-1′,2′-$C_2B_9H_{10}$)], is reported. Biodistribution studies in rodents using dissection/gamma counting and *in vivo* nuclear imaging have been performed. The general strategy reported here can be applied in the future to COSAN derivatives bearing a wide range of functionalities.

Abnormal metabolism and over-expression of membrane receptors in cancer cells have been historically exploited to deliver therapeutic amounts of boron into tumours using boronated carbohydrate,[1] amino acid, peptide,[2] and nucleic acid derivatives,[3] and immunoconjugates.[4] With the emergence of nanotechnology, drug delivery systems such as liposomes, which may passively accumulate in the tumour, thanks to the enhanced permeability and retention (EPR) effect, have gained attention.[5]

The inorganic, boron-based molecule cobaltabisdicarbollide, $[3,3'\text{-Co}(1,2\text{-}C_2B_9H_{11})_2]^-$, commonly known as COSAN (Fig. 1), is a stable complex in which the cobalt atom is sandwiched between two η^5-bonding $[C_2B_9H_{11}]^{2-}$ moieties.[6] While showing differentiated properties from lipid molecules (*e.g.* amphiphilic character in water),[7] COSAN has the ability to assemble into monolayer vesicles.[8] As recently demonstrated by us, COSAN can cross through synthetic lipid membranes without disrupting membrane integrity[9] and accumulates *in vitro* within living cells.[10] Additionally, it can be readily multi-decorated by incorporation of functional groups into the different vertices. These properties, together with its high boron content, chemical stability and solubility under physiologic conditions,[6] make COSAN a suitable building block for the preparation of boron carrier drugs.

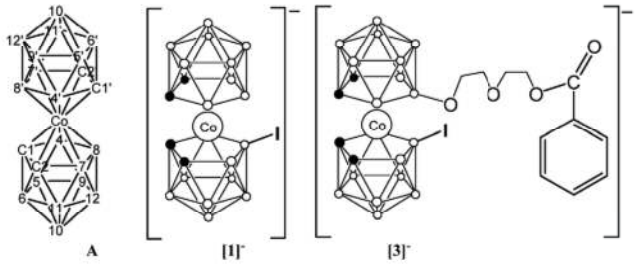

Fig. 1 Vertex numbering of the anionic COSAN cluster (A) and its iodinated derivatives $[3,3'\text{-Co}(8\text{-I-}1,2\text{-}C_2B_9H_{10})(1',2'\text{-}C_2B_9H_{11})]^-$, **[1]**$^-$ and $[3,3'\text{-Co}(8\text{-I-}1,2\text{-}C_2B_9H_{10})(8'\text{-}(OCH_2CH_2)_2COOC_6H_5\text{-}1',2'\text{-}C_2B_9H_{10})]^-$, **[3]**$^-$, respectively.

Despite the large variety of COSAN derivatives being described in the literature with potential application in boron neutron capture therapy (BNCT), the transition from bench to bed (even in the preclinical setting) has been only occasionally approached. The main reason behind this fact still remains the lack of techniques able to determine, *in vivo* and in real time, the accumulation of boron in the tumour and surrounding tissues, allowing a candidate-by-candidate screening and prediction of therapeutic efficacy. Nuclear imaging techniques such as Positron Emission Tomography (PET) and Single Photon Emission Computerized Tomography (SPECT) in combination with X-ray Computed Tomography (CT) are valuable tools for the *in vivo* assessment of pharmacokinetic properties of new chemical entities;[11] they are thus anticipated to be suitable methods for determining boron accumulation in the tumour and surrounding tissues. Nonetheless, application of nuclear imaging requires radiolabelling of the molecule under investigation with a positron or a gamma emitter.[12] To date and to the best of our knowledge, radiolabelling of polyhedral boranes and heteroboranes with the radionuclide covalently attached to the cluster cage has been restricted to *nido* and *closo* derivatives.[13]

In this communication, the synthesis of a new bi-functional (iodine and polyethylene glycol, PEG) COSAN derivative and its unprecedented radiolabelling with either ^{125}I (gamma emitter) or ^{124}I (positron emitter) *via* a palladium catalyzed isotopic exchange reaction are reported. Incorporation of ^{125}I and ^{124}I enabled the

[a] *Radiochemistry and Nuclear Imaging, CIC biomaGUNE, Paseo de Miramón 182, 20009 Donostia, San Sebastian, Spain. E-mail: jllop@cicbiomagune.es; Fax: +34 94 3005301*

[b] *Institut de Ciència de Materials de Barcelona (ICMAB-CSIC), Campus de la U.A.B., E-08193 Bellaterra, Spain. E-mail: clara@icmab.es; Fax: +34 93 5805729*

† Electronic supplementary information (ESI) available. See DOI: 10.1039/c4cc05058d

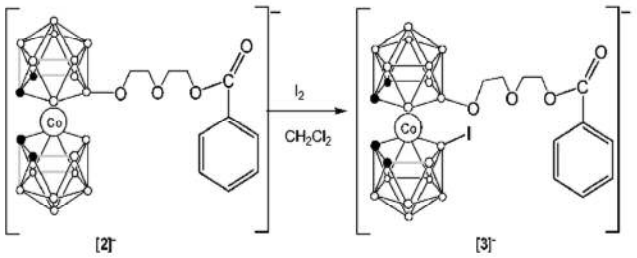

Scheme 1 Synthesis of a mixed doubly functionalized derivative of COSAN.

determination of the biodistribution pattern by using dissection/gamma counting and PET-CT, respectively. Comparison with its parent I-COSAN, $[3,3'\text{-}Co(8\text{-}I\text{-}1,2\text{-}C_2B_9H_{10})(1',2'\text{-}C_2B_9H_{11})]^-$, was also carried out. The general strategy reported here should be suitable for the radiolabelling of specifically targeted COSAN derivatives, enabling their evaluation *in vivo* and facilitating translation into the clinical setting.

First, and with the aim of generating mixed-doubly functionalized COSAN derivatives simultaneously incorporating two markedly different reactive sites (*i.e.* a PEG branch and a suitable moiety for subsequent incorporation of the radioisotope), the synthesis of $[3,3'\text{-}Co(8\text{-}I\text{-}1,2\text{-}C_2B_9H_{10})(8'\text{-}(OCH_2CH_2)_2COOC_6H_5\text{-}1',2'\text{-}C_2B_9H_{11})]^-$, $[\mathbf{3}]^-$, was carried out (Scheme 1). In brief, to a solution of 225 mg (0.39 mmol) of $Na[3,3'\text{-}Co(8\text{-}(OCH_2CH_2)_2COOC_6H_5\text{-}1,2\text{-}C_2B_9H_{11})(1,2\text{-}C_2B_9H_{11})]$, Na[**2**],[14] in 10 mL of reagent grade CH_2Cl_2, 200 mg of iodine (0.78 mmol) were added. The reaction mixture was left to stand overnight at room temperature and then heated under reflux for 1.5 h. The excess iodine was quenched with aqueous Na_2SO_3 solution, the resulting mixture was evaporated, and the orange solid was washed with water before being extracted with diethyl ether (3 × 10 mL). After drying over anhydrous $MgSO_4$, the organic layer was evaporated to obtain Na[**3**] in 81% yield.

The MALDI-TOF analysis showed the desired molecular peak at 659.28 *m/z* corresponding to M (100%) and a fragmentation peak at 553.26 (M-I, 6%). The IR spectra showed bands at 3040, 2947–2869, 2568–2539, 1736 and 1100–1071 cm^{-1} corresponding to C_c–H, C_{alkyl}–H, B–H, C–O and O–C–O, respectively.

Radiolabelling reactions on compounds $[\mathbf{1}]^-$ and $[\mathbf{3}]^-$ were performed by adapting the previously reported palladium catalyzed iodine exchange reaction on iodinated dicarba-*closo*-dodecaborane.[13b] Experimental conditions were first optimized using ^{125}I, which is a convenient radioisotope due to its long half-life (59.4 d) and low cost. With this aim, the precursors ($[\mathbf{1}]^-$ and $[\mathbf{3}]^-$, 2.6 μmol) were reacted with 740 KBq (20 μCi) of $Na[^{125}I]I$ (solution in 0.1 M aqueous NaOH) in the presence of Hermann's catalyst (0.1 mg) (Scheme 2). Radiochemical conversion values close to 85% were achieved for compound $[\mathbf{1}]^-$ when the reaction was conducted at 100 °C for 3 min, as determined by high performance liquid chromatography (HPLC) using radiometric detection; longer reaction times did not improve radiochemical conversion. For compound $[\mathbf{3}]^-$, the formation of unidentified labelled species was detected when the reaction was conducted at 100 °C. Lower reaction temperatures (80 °C) led to almost 80% radiochemical conversion after 8 min. Again, longer reaction times yielded lower incorporation yields, suggesting the degradation of the precursor and the

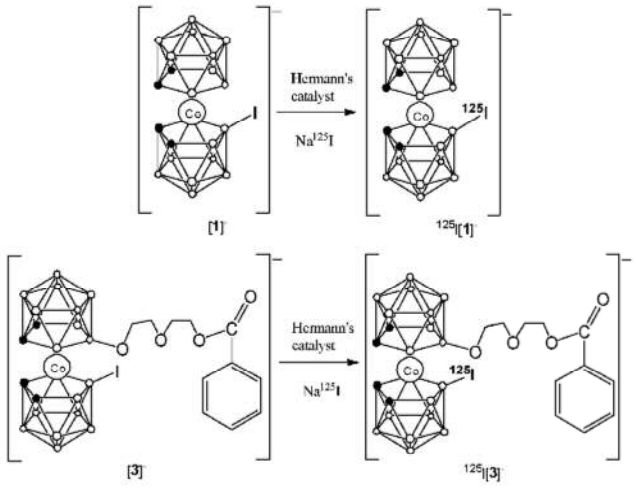

Scheme 2 Radioiodination reaction of mono anionic species ^{125}I-$[\mathbf{1}]^-$ (top) and ^{125}I-$[\mathbf{3}]^-$ (bottom). Reaction conditions for $[\mathbf{1}]^-$: $Na[^{125}I]I$, Hermann's catalyst, toluene, 100 °C, 3 min. Reaction conditions for $[\mathbf{3}]^-$: $Na[^{125}I]I$, Hermann's catalyst, toluene, 80 °C, 8 min.

radiolabelled compound. Purification by semi-preparative HPLC followed by solvent evaporation and reconstitution with C_2H_5OH–H_2O (1/9) resulted in injectable solutions of chemically and radiochemically pure compounds (see Fig. S1, ESI† for an example of a chromatographic profile).

Lipophilicity of the radiolabelled compounds was calculated by the distribution coefficient (Log *D*). Log *D* values of 1.1 ± 0.1 and 1.5 ± 0.1 were obtained for ^{125}I-$[\mathbf{1}]^-$ and ^{125}I-$[\mathbf{3}]^-$, respectively. These results indicate that the presence of the PEG arm in $[\mathbf{3}]^-$ results in a slight increase in the lipophilicity.

Biodistribution studies using dissection and gamma counting were performed in mice. The amount of radioactivity in the different organs was determined at three time points after administration of the radiolabelled species (10, 30 and 120 minutes, Fig. 2a and b).

Very similar patterns were obtained for both compounds: high accumulation in the liver throughout the duration of the study, increasing uptake in the lungs and moderate blood clearance. Uptake in the kidneys and the spleen was also significant and lower accumulation was detected in other organs. Progressive accumulation in the intestine and the low concentration of radioactivity in the bladder (urine) suggest biliary excretion.

Moving towards *in vivo* application, the incorporation of the positron emitter ^{124}I was approached; with that aim, the radiolabelling process was performed following the optimized experimental conditions developed for ^{125}I, with equivalent incorporation ratios.

In vivo PET studies were conducted in combination with CT (Fig. 2c and d),‡ the latter for anatomical localization of the volumes of interest (VOIs). PET acquisitions were started concomitantly with the administration of the radiolabelled ^{124}I-$[\mathbf{1}]^-$ and ^{124}I-$[\mathbf{3}]^-$ species, and dynamic images were acquired (20 frames, total acquisition time of 130 min). In this case, only those organs clearly visualized on the CT images (lungs, heart, kidneys, liver, intestine, brain, bladder and stomach) were analyzed (Fig. S2 and S3, ESI†). A good correlation between results obtained using both methodologies (*in vivo* imaging and dissection/gamma counting) was obtained (Fig. 2e and Fig. S4, ESI†), although significant differences were observed at different

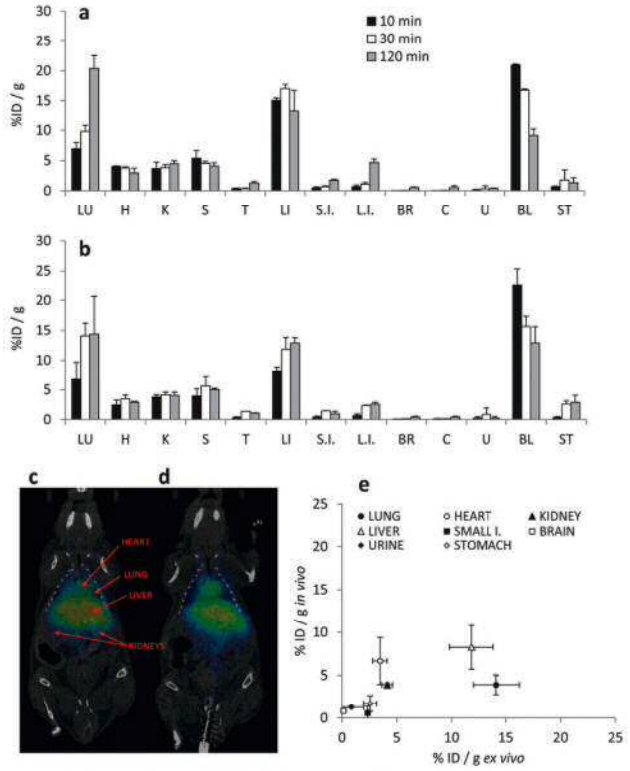

Fig. 2 Biodistribution of ^{125}I-[**1**]$^-$ (a) and ^{125}I-[**3**]$^-$ (b) in mice tissues (mean ± standard deviation, n = 3) using the dissection method. Radioactivity is expressed as the percentage of the injected dose (ID) per gram of tissue. LU: lungs; H: heart; K: kidneys; S: spleen; T: testicles; L: liver; S.I.: small intestine; L.I.: large intestine; BR: brain; C: cerebellum; U: urine; BL: blood; ST: stomach; (c and d) PET coronal projections resulting from averaged images (frames 12–20) obtained after administration of ^{124}I-[**1**]$^-$ (c) and ^{124}I-[**3**]$^-$ (d). Co-registration with CT images of the same animal is shown; (e) correlation between results obtained using PET-CT (expressed as %ID cm^{-3} of tissue) and dissection and gamma counting (expressed as %ID g^{-1} of tissue) for compound ^{125}I-[**3**]$^-$ at 30 minutes after administration.

time points in the brain, the bladder and the lungs. As a general trend, higher accumulation values in the brain were obtained *in vivo*, probably due to the contribution of the blood to the overall quantification of the uptake in this region. In the particular case of the lungs, the differences can be attributed to the fact that the percentage of injected dose (%ID) per gram of tissue is measured *ex vivo*, whereas *in vivo*, the %ID per cm^3 is obtained. Because the density of the lungs significantly differs from 1 g cm^{-3}, the results obtained in both experiments cannot be directly compared. Differences observed in the bladder might be due to urination during image acquisition (*in vivo*) or uptake time (*ex vivo*). Interestingly, *in vivo* studies did not show accumulation of radioactivity in the thyroid gland, suggesting the stability of both ^{124}I-[**1**]$^-$ and ^{124}I-[**3**]$^-$.

A new bifunctional COSAN derivative incorporating a PEG arm and one iodine atom has been synthesized and successfully radiolabelled with ^{124}I and ^{125}I *via* palladium catalyzed iodine exchange. The biodistribution pattern of the radiolabelled cobaltabisdicarbollide species has been determined using dissection/gamma counting and real-time, *in vivo* and noninvasive imaging (PET-CT). The general radiolabelling strategy reported here, which can be applied in the future to COSAN derivatives bearing a wide range of functionalities, might be applicable to targeted cobaltabisdicarbollides able to selectively accumulate in tumors. Hence, our method may become an invaluable, widely applied tool for the fast and accurate evaluation of new COSAN-based BNCT drug candidates in animal tumor models. Due to the noninvasive nature of PET imaging, potential translation into the clinical setting to predict therapeutic efficacy on a patient-by-patient basis can also be foreseen.

This work was supported by Generalitat de Catalunya (2009/SGR/ 00279) and Spanish Ministry of Economy and Competitiveness (CTQ2010-16237). A. Z. is enrolled in the PhD program of the UAB. The authors would like to thank Maria Puigivila for assistance in experimental work involving animals and Zuriñe Baz for image analysis.

Notes and references

‡ The animals were maintained and handled in accordance with the Guidelines for Accommodation and Care of Animals (European Convention for the Protection of Vertebrate Animals Used for Experimental and Other Scientific Purposes) and internal guidelines. Experimental procedures were approved by local authorities.

1 (*a*) S. Ronchi, D. Prosperi, C. Thimon, C. Morin and L. Panza, *Tetrahedron: Asymmetry*, 2005, **16**, 39; (*b*) S. Stadlbauer, P. Welzel and E. Hey-Hawkins, *Inorg. Chem.*, 2009, **48**, 5005; (*c*) S. Stadlbauer, P. Loennecke, P. Welzel and E. Hey-Hawkins, *Eur. J. Org. Chem.*, 2010, 3129.
2 (*a*) V. M. Ahrens, R. Frank, S. Stadbauer, A. G. Beck-Sickinger and E. Hey-Hawkins, *J. Med. Chem.*, 2011, **54**, 2368; (*b*) M. Yu. Stogniy, M. V. Zakharova, I. B. Sivaev, I. A. Godovikov, A. O. Chizov and V. I. Bregadze, *Polyhedron*, 2013, **55**, 117; (*c*) C. Morin and C. Thimon, *Eur. J. Org. Chem.*, 2004, 3828.
3 (*a*) S. Hasabelnaby, A. Goudah, H. K. Agarwal, M. S. M. Abdalla and W. Tjarks, *Eur. J. Med. Chem.*, 2012, **55**, 325; (*b*) A. Semioshkin, A. Ilinova, I. Lobanova, V. Bregadze, E. Paradowska, M. Studzińska, A. Jabłońska and Z. J. Lesnikowski, *Tetrahedron*, 2013, **37**, 8034.
4 W. Yang, R. F. Barth, G. Wu, W. Tjarks, P. Binns and K. Riley, *Appl. Radiat. Isot.*, 2009, **67**(7–8), S328.
5 (*a*) K. Maruyama, O. Ishida, S. Kasaoka, T. Takizawa, N. Utoguchi, A. Shinohara, M. Chiba, H. Kobayashi, M. Eriguchi and H. J. Yanagie, *J. Controlled Release*, 2004, **98**, 195; (*b*) H. Koganei, M. Ueno, S. Tachikawa, L. Tasaki, H. S. Ban, M. Suzuki, K. Shiraishi, K. Kawano, M. Yokoyama, Y. Maitani, K. Ono and H. Nakamura, *Bioconjugate Chem.*, 2013, **24**, 124; (*c*) S. Masunaga, S. Kasaoka, K. Maruyama, D. Nigg, Y. Sakurai, K. Nagata, M. Suzuki, Y. Kinashi, A. Maruhashi and K. Ono, *Int. J. Radiat. Oncol., Biol., Phys.*, 2006, **66**, 1515; (*d*) X. Pan, G. Wu, W. Yang, R. F. Barth, W. Tjarks and R. J. Lee, *Bioconjugate Chem.*, 2007, **18**, 101; (*e*) M. Ueno, H. S. Ban, K. Nakai, R. Inomata, Y. Kaneda, A. Matsumura and H. Nakamura, *Bioorg. Med. Chem.*, 2010, **18**(9), 3059.
6 N. Grimes, *Carboranes*, Academic Press, Burlington, MA, 2011.
7 P. Matějíček, P. Cígler, K. Procházka and V. Král, *Langmuir*, 2006, **22**, 575.
8 P. Bauduin, S. Prevost, P. Farras, F. Teixidor, O. Diat and T. Zemb, *Angew. Chem., Int. Ed.*, 2011, **50**, 5298.
9 C. Verdiá-Báguena, A. Alcaraz, V. M. Aguilella, A. M. Cioran, S. Tachikawa, H. Nakamura, F. Teixidor and C. Viñas, *Chem. Commun.*, 2014, **50**(51), 6677.
10 M. Tarrés, E. Canetta, C. Viñas, F. Teixidor and A. J. Harwood, *Chem. Commun.*, 2014, **50**(51), 3370.
11 M. D. Bartholomä, A. S. Louie, J. F. Valliant and J. Zubieta, *Chem. Rev.*, 2010, **110**(5), 2903.
12 S. Achilefu, *Chem. Rev.*, 2010, **110**(5), 2575.
13 (*a*) V. Tolmachev, A. Bruskin, I. Sivaev, H. Lundqvist and S. Sjöberg, *Radiochim. Acta*, 2002, **90**, 229; (*b*) K. J. Winberg, G. Barberà, L. Eriksson, F. Teixidor, V. Tolmachev, C. Viñas and S. Sjöberg, *J. Organomet. Chem.*, 2003, **680**, 188; (*c*) D. S. Wilbur, D. K. Hamlin, R. R. Srivastava and M. K. Chyan, *Nucl. Med. Biol.*, 2004, **31**, 523; (*d*) M. E. El-Zaria, N. Janzen, M. Blacker and J. F. Valliant, *Chem. – Eur. J.*, 2012, **18**(35), 11071; (*e*) K. B. Gona, V. Gómez-Vallejo, D. Padro and J. Llop, *Chem. Commun.*, 2013, **49**, 11491.
14 P. Farràs, F. Teixidor, R. Kivekäs, R. Sillanpää, C. Viñas, B. Grüner and I. Cisarova, *Inorg. Chem.*, 2008, **47**(20), 9497.

Journal of Organometallic Chemistry 747 (2013) 229–234

Contents lists available at ScienceDirect

Journal of Organometallic Chemistry

journal homepage: www.elsevier.com/locate/jorganchem

Investigations on antimicrobial activity of cobaltabisdicarbollides

Teodora Popova [a], Adnana Zaulet [b,1], Francesc Teixidor [b], Radostina Alexandrova [c], Clara Viñas [b,*]

[a] Faculty of Veterinary Medicine, Forestry Technical University, 10 Kliment Ohridski Blvd, 1756 Sofia, Bulgaria
[b] Institut de Ciència de Materials de Barcelona (CSIC), Campus de la UA.B, E-08193 Bellaterra, Spain
[c] Institute of Experimental Morphology, Pathology and Anthropology with Museum, Bulgarian Academy of Sciences, Acad. Georgi Bonchev Str., Block 25, Sofia 1113, Bulgaria

ARTICLE INFO

Article history:
Received 12 April 2013
Received in revised form
26 June 2013
Accepted 2 July 2013

Dedicated to Prof. Vladimir Bregadze on the occasion to his 75th anniversary in recognition to his outstanding contribution to Boron clusters compounds.

Keywords:
Antimicrobial
Antifungal activity
Metallacarboranes

ABSTRACT

Metallacarboranes have been identified as promising pharmacophores and building blocks in drug designed as well as inhibitors of HIV. The aim of this study was to evaluate the putative antimicrobial properties *in vitro* of cobaltabisdicarbollide [3,3′-Co(1,2-$C_2B_9H_{11}$)$_2$]$^-$, H[**1**], and its derivatives [3,3′-Co(8-R(CH_2CH_2O)$_2$-1,2-$C_2B_9H_{10}$)(1′,2′-$C_2B_9H_{11}$)]$^-$ (R = $-OOCCH_3$ (Na[**3**]); $-OCH_3$ (Na[**6**]); $-OCH_2CH_3$ (Na[**7**])). Pure cultures of 16 pathogenic bacterial strains (isolated from animals and humans as well as control strains) and 3 strains of *Candida* spp. were applied in antimicrobial studies that were performed by the agar-diffusion method of Bauer–Kirby and the method of minimum inhibitory concentrations. The obtained results revealed that among the compounds examined Na[**7**] and Na[**4**] exhibited the highest antimicrobial activity that was equal or even higher than those of the commercially available broad-spectrum antibiotic thiamphenicol. The cobaltabisdicarbollide H[**1**] was shown to express comparatively lower antibacterial and antifungal properties as compared to its derivatives. From a practical point of view it is important to emphasize that the meticillin-resistant strain of *Staphylococcus aureus* (TSA MRSA), the poliresistant strains of *Pseudomonas aeruginosa*, as well as of *Candida* spp., are sensitive to the compounds Na[**7**] and Na[**4**].

1. Introduction

Recently, there is an increasing interest in biological activity and medicinal application of boron and boron compounds [1]. Boron compounds (boronic acids, boron heterocycles, etc.) are reported to be promising antibacterials [2] and antifungal agents [3]. There are data that some curcumin boron complexes [4], boronic acid compounds [5], boron-modified polypeptides [6] and metallocarboranes [7] are specific and potent inhibitors of HIV protease.

The anionic *closo* icosahedral cobaltabisdicarbollide [3,3′-Co(1,2-$C_2B_9H_{11}$)$_2$], [**1**]$^-$, that show great chemical stability, electrochemical activity, high volume, low nucleophilic character, low charge density and amphiphilic properties [8] has been the object of many studies [9] since its discovery in 1968 [10]. Their derivatives are highly air-stable, very robust, withstanding strong acid, moderate base, high temperatures and intense radiation [9a]. The cobaltabisdicarbollide [**1**]$^-$ has been proposed in a wide range of applications such as extraction of radionuclides [11], conducting organic polymers [12] or use in medicine [13]. The use of polyhedral boron hydrides for cancer treatment is traditionally connected with a binary approach for cancer treatment named Boron Neutron Capture Therapy (BNCT) [14].

Polyhedral metallaborane and metallacarborane anions were proposed as carriers of radionuclide label for targeted radionuclide therapy/diagnostics of cancer [15] and several of them were found to demonstrate significant antitumor activity themselves [15,16].

There is a significant global need for new antibacterial and alternative mechanisms of action given the rise in resistance among bacteria [17]. The chemical and biological stability, low toxicity, and the possibility to introduce various modifications make boron clusters and specially H[**1**] attractive pharmacophores for potent and specific enzyme inhibition. The aim of this study is to expand the biomedical applications by evaluating the putative antimicrobial properties of the salts H[**1**], Na[**3**] to Li[**8**].

* Corresponding author. Tel.: +34 93 5801853, +34 93 5805729; fax: +34 93 5805729.
E-mail addresses: teixidor@icmab.es (F. Teixidor), rialexandrova@hotmail.com (R. Alexandrova), clara@icmab.es (C. Viñas).
[1] Adnana Zaulet is enrolled in the UAB PhD program.

0022-328X/$ – see front matter © 2013 Elsevier B.V. All rights reserved.
http://dx.doi.org/10.1016/j.jorganchem.2013.07.006

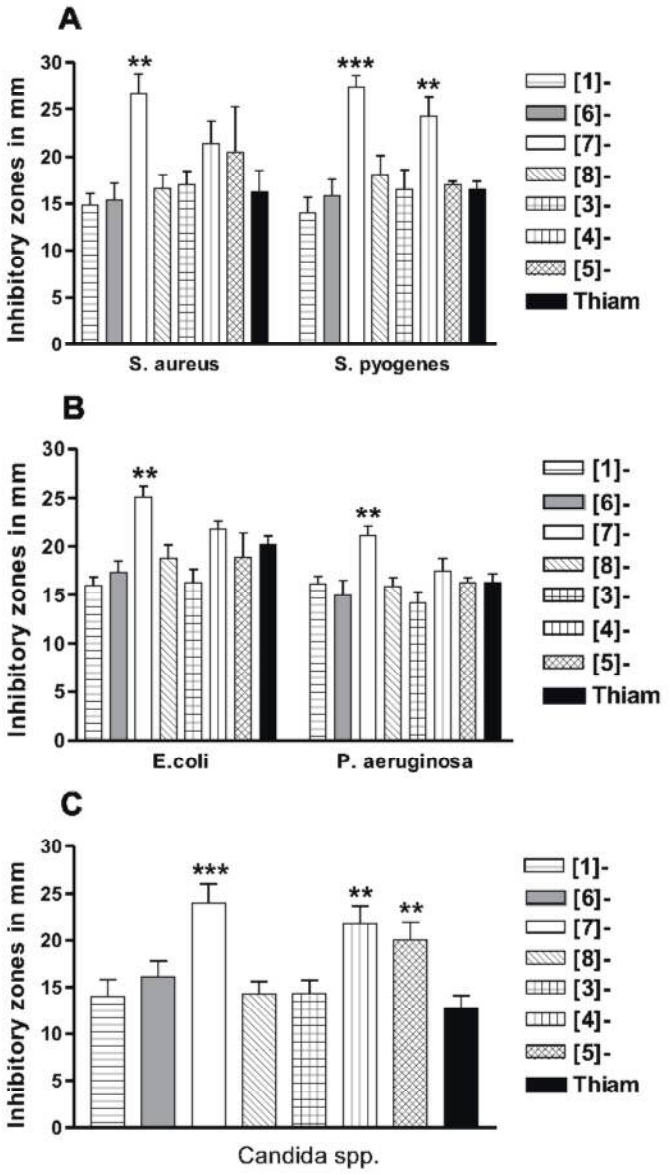

Fig. 1. Inhibitory effects of newly synthesized cobaltabisdicarbollides on pathogenic microorganisms: Gram-positive bacteria (A), Gram-negative bacteria (B) and *Candida* spp. fungi (C). Significant differences versus wide-spectrum antibiotic thiamphenicol (used as positive control) are presented: $^{*}P < 0.05$; $^{**}P < 0.01$; $^{***}P < 0.001$ vs. thiamphenicol (Thiam); $n = 5$; being n the number of independent experiments performed *in vitro*.

2. Experimental section

2.1. Materials

2.1.1. Chemicals

Dimethyl sulfoxide (DMSO) neutral red and trypsin were purchased from AppliChem (Darmstadt, Germany); Mueller–Hinton's agar was from Scharlau Chemie S.A. (Barcelona, Spain). Dulbecco's modified Eagle's medium (D-MEM) and fetal bovine serum were from Gibco-Invitrogen (UK); thiazolyl blue tetrazolium bromide (MTT) was obtained from Sigma–Aldrich Chemie GmbH (Germany). All other chemicals of the highest purity commercially available were purchased from local agents and distributors. All sterile plasticware and syringe filters were from Orange Scientific (Belgium).

Synthesis of Cobaltabisdicarbollide compounds: Following our studies on cobaltabisdicarbollides' direct substitution, we recently reported on the high yield synthesis of polyanionic species as novel high-boron content molecules with enhanced water solubility [18]. The synthetic ways were based on the use of carboxylates and alkoxides as nucleophiles in the ring-opening reaction of cyclic oxonium $[3,3'\text{-}Co(8\text{-}C_4H_8O_2\text{-}1,2\text{-}C_2B_9H_{10})(1',2'\text{-}C_2B_9H_{11})]$, **[2]** compound [19]. We have synthesized sodium salts that incorporate a PEG chain and the $[3,3'\text{-}Co(1,2\text{-}C_2B_9H_{11})_2]^-$ moiety. Chart 1 shows the species $Na(H_2O)[3,3'\text{-}Co(8\text{-}O(CH_2CH_2O)_2C(O)CH_3\text{-}1,2\text{-}C_2B_9H_{10})(1',2'\text{-}C_2B_9H_{11})]$, Na[**3**]; $Na[1''\text{-}\{3,3'\text{-}Co(8\text{-}O(CH_2CH_2O)_2C(O)\text{-}1,2\text{-}C_2B_9H_{10})(1',2'\text{-}C_2B_9H_{11})\}\text{-}2''\text{-}OH\text{-}C_6H_4]$, Na[**4**]; $Na_3[1'',3'',5''\text{-}\{3,3'\text{-}Co(8\text{-}O(CH_2CH_2O)_2\text{-}1,2\text{-}C_2B_9H_{10})(1',2'\text{-}C_2B_9H_{11})\}_3\text{-}C_6H_3]$, Na_3[**5**]; $Na[3,3'\text{-}Co(8\text{-}O(CH_2CH_2O)_2CH_3\text{-}1,2\text{-}C_2B_9H_{10})(1',2'\text{-}C_2B_9H_{11})]$, Na[**6**]; $Na[3,3'\text{-}Co(8\text{-}O(CH_2CH_2O)_2CH_2CH_3\text{-}1,2\text{-}C_2B_9H_{10})(1',2'\text{-}C_2B_9H_{11})]$, Na[**7**] that were synthesized from the zwitterionic **[2]** according to Scheme 1 following the reported procedure [18a,19a]. The chelating ligand derivative $Li[1,1'\text{-}(PPh_2)_2\text{-}3,3'\text{-}Co(1,2\text{-}C_2B_9H_{10})_2]$, Li[**8**], was synthesized (see Scheme 2) in one pot reaction in very good yield and with an easy working up process according to the method reported at the literature [20].

The cobaltabisdicarbollide species were dissolved in DMSO and diluted in sterile PBS for antibacterial tests or in culture medium for cytotoxicity investigations. The final concentration of DMSO in the stock solutions (where the concentration of the tested compound was 1 mg/mL) was 2%. It has been recently reported [21] that metallacarboranes are often poorly soluble in water and have the tendency to aggregate in aqueous media but it has not been observed in this study.

The commercially available broad spectrum antibiotic thiamphenicol was applied in antimicrobial investigations as a positive control. The dilutions of the antibiotic were prepared in sterile PBS.

2.1.2. Microorganisms

The antimicrobial activity of the compounds was tested on a broad range of Gram-positive and Gram-negative pathogenic bacterial strains (isolated either from animals or humans as well as the control strains) and on *Candida* spp. In our experiments we used 4 strains of *Staphylococcus aureus* (*S. aureus* TSA MRSA, *S. aureus* Kowan, *S. aureus* 131, *S. aureus* 230), 4 of *Streptococcus pyogenes* (*S. pyogenes* 1, *S. pyogenes* 2, *S. pyogenes* 184, *S. pyogenes* 383), 4 of *Escherichia coli* (*E. coli* 045, *E. coli* 075-20, *E. coli* 16 − B, *E. coli* 0621 − C) and 4 of *Pseudomonas aeruginosa* (*P. aeruginosa* 1, *P. aeruginosa* 177, *P. aeruginosa* 318, *P. aeruginosa* 357). The bacterial strains were isolated from patients with infections of different location (skin, ears, conjunctiva, respiratory and urogenital tracts) that were subject to continuous treatment with various antibacterial means. The strains showed *in vitro* a high drug resistance mainly to streptomycin, penicillin, oxacillin, ampicillin, and some of them also to amoxicillin but are sensitive to amphenicols (established by the agar-diffusion method of Bauer–Kirby in the Laboratory of Microbiology, Faculty of Veterinary Medicine, Forest Technical University, Sofia, Bulgaria).

Pure cultures of 3 pathogenic strains of *Candida albicans* (*C. albicans* 1, *C. albicans* 332, *C. albicans* 398) and 1 of *Candida tropicalis* (*C. tropicalis* 324) were also included in the experiments.

2.1.3. Animal cell cultures

Madin–Darby bovine kidney (MDBK) non-tumor permanent cell line was used in our investigations. The cells were grown as monolayer culture in D-MEM medium, supplemented with 5–10% fetal bovine serum, 100 U/mL penicillin and 100 μg/ml streptomycin. The cultures were maintained at 37 °C in a humidified CO_2 incubator. For routine passages, adherent cells were detached using a mixture of 0.05% trypsin and 0.02% EDTA. The experiments were performed during the exponential phase of cell growth.

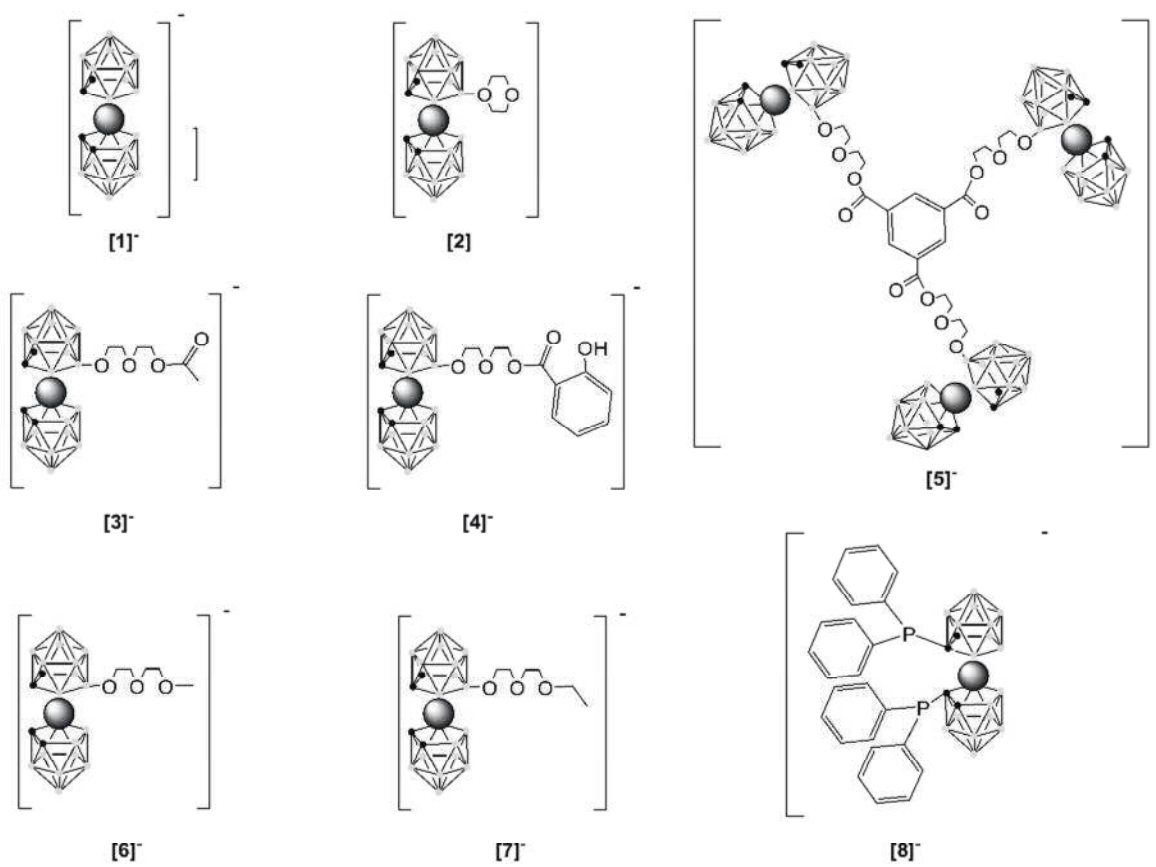

Chart 1. Monosubstituted cobaltabisdicarbollide anions.

2.2. Methods

2.2.1. Antimicrobial tests

Studies were carried out by the classic agar-diffusion method of Bauer–Kirby [22]. Bacterial suspensions were inoculated at a concentration of 2×10^6 cells/mL on Mueller–Hinton's agar with pH 7.2–7.4 and 4 mm layer thickness in Petri dishes with diameter 9 cm. The compounds and controls were applied as phosphate-saline solutions by dropping of 0.1 mL in 9-mm holes in the agar that correspond to an amount of 50 μg/well for the compounds and 30 μg/well for the antibiotic. Results were recorded after 24 h incubation period by measuring the diameters of inhibitory zones in mm, including the hole diameter. Inhibitory effect of the cobaltabisdicarbollides was established at zones >12 mm.

The determination of the minimum inhibitory concentrations (MICs) that inhibits 50% (MIC_{50}) and 90% (MIC_{90}) of the treated microorganisms [23,24], was performed by the method of two-fold serial dilutions on Mueller–Hinton's agar as reported [25]. The determination of the minimum inhibitory concentrations (MICs) was performed by the method of two-fold serial dilutions on Mueller–Hinton's agar as reported [25].

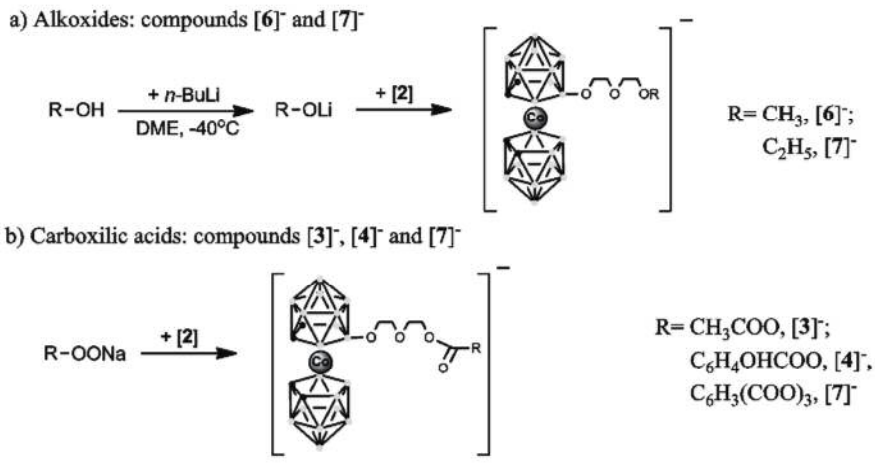

Scheme 1. Opening of the *exo*-cluster dioxanate ring reaction by nucleophilic attack. Atoms in black are CH vertexes, the rest of the vertices in the clusters are BH or BO.

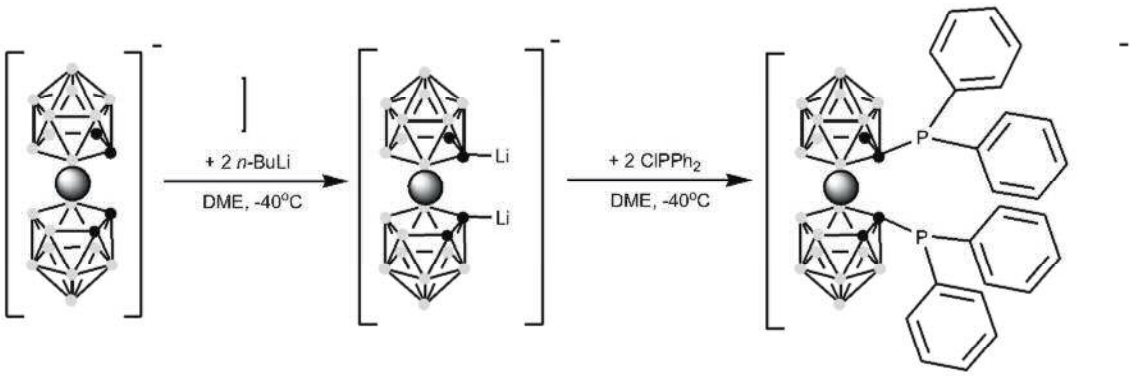

Scheme 2. - Synthesis of Li[**8**].

Since the tested compounds are synthetic and not antibiotics, their dosages were determined between these of the antibiotic (30 μg of thiamphenicol) and chemotherapeutic agents such as sulfonamides and others (250 or 300 g). MIC_{50} were calculated mathematically depending on the number of inhibited colonies of the medium with the respective compound or antibiotic dilution compared to the control medium colonies without drugs. According to Rodríguez-Argüelles et al. [26], the experiments with the compounds with absence of antimicrobial activity was recorded at $MIC_{50} > 100$ μg/ml, and the antimicrobial effect at $MIC_{50} < 100$ μg/ml. The effect of the tested compounds is determined as high at $MIC_{50} < 50$ μg/ml.

2.2.2. Cytotoxicity assays

The cells were seeded in 96-well flat-bottomed microplates at a concentration of 1×10^4 cells/well. After the cells were grown for 24 h to a subconfluent state (~60–70%), the cells from monolayers were washed with phosphate-buffered saline (PBS, pH 7.2) and covered with media modified with different concentrations (5, 10, 20, 50 and 100 μg/ml) of the compounds tested. Each solution was applied into 4 to 6 wells. Samples of cells grown in non-modified medium served as controls. After 72 h of incubation, the effect of the compounds on cell viability and proliferation was examined by MTT (thiazolyl blue tetrazolium bromide) test and neutral red uptake cytotoxicity assay (NR).

The MTT colorimetric assay of cell survival was performed as described by Mossman (1983) [27]. The method consisted of 3 h incubation with MTT solution (5 mg MTT in 10 mL D-MEM) at 37 °C under 5% carbon dioxide and 95% air, followed by extraction with a mixture of absolute ethanol and DMSO (1:1, vol/vol) to dissolve the blue MTT formazan.

The NR assay was based on the method of Borenfreund and Puerner (1885) [28]. Briefly, to each well medium containing 50 μg NR/mL (0.1 mL) was added. The plate was placed in the incubator for 3 h for the uptake of the vital dye. Thereafter, the medium with NR was removed and the cells were washed with phosphate-buffered saline (0.2 mL/well), followed by the addition of 0.1 mL 1% acetic acid solution containing 50% ethanol to extract the dye from the cells.

Optical density was measured at 540 nm (MTT, NR) using an automatic microplate reader (TECAN, Sunrise™, Austria). Relative cell viability, expressed as a percentage of the untreated control (100% viability), was calculated for each concentration. "Concentration–response" curves were prepared and the effective concentrations of the compounds – CC_{50} (causing a 50% reduction of cell viability) were estimated (where possible) from these curves using Origin 6.1. All data points represent an average of three independent assays.

2.2.3. Statistical analysis

The data are presented as mean ± standard error of the mean. Statistical differences between control and treated groups were assessed using one-way analysis of variance (ANOVA) followed by Dunnett post-hoc test and Origin 6.1™ in some cases.

3. Results and discussion

The results obtained by the agar-gel diffusion method are presented in Fig. 1. They revealed that the compounds examined expressed antibacterial activity against both Gram-positive (Fig. 1A) and Gram-negative (Fig. 1B) bacteria that is comparable or better (in the case of Na[**7**]) than those of the wide-spectrum potent antibiotic thiamphenicol, used as a positive control.

According to their antibacterial properties (the diameter of the inhibitory zones) the most effective cobaltabisdicarbollides were Na[**7**], Na[**4**] and Na_3[**5**]. The same compounds manifested also significant antifungal activity *in vitro* (Fig. 1C). The meticillin-resistant strain of *S. aureus* (TSA MRSA), the poliresistant strains

Table 1
Minimum inhibitory concentration (MIC) of cobaltabisdicarbollide complexes on pathogenic microorganisms.

Microorganism	Number of strains	MIC_{50}				
		Na[**7**]	Li[**8**]	Na[**4**]	Na_3[**5**]	Thiam.
S. aureus	4	12.8 ± 7.3	36.0 ± 10.1	10.1 ± 7.3	48.0 ± 9.2	21.3 ± 6.2
S. pyogenes	4	3.1 ± 1.6*	26.0 ± 6.0	2.5 ± 0.6**	48.0 ± 9.2	20.0 ± 9.9
E. coli	4	7.0 ± 1.0*	26.0 ± 6.0	4.0 ± 0.1*	22.0 ± 6.0	12.0 ± 2.3
P. aeruginosa	4	18.0 ± 5.0	22.0 ± 6.0	8.0 ± 2.8*	17.0 ± 5.7	20.5 ± 3.8
Candida spp.	4	1.4 ± 0.2***	28.0 ± 4.0	2.3 ± 0.4***	32.0 ± 0.1	14.0 ± 2.0

Significantly lower MICs versus wide-spectrum antibiotic thiamphenicol (used as positive control) are presented as follows: *$P < 0.05$, **$P < 0.01$, ***$P < 0.001$ vs. thiamphenicol.

of *P. aeruginosa*, as well as of *Candida* spp., showed sensitivity to these three compounds.

The investigations of the most active antimicrobial substances were continued with the determination of their minimal inhibitory concentrations (MICs), which are presented in Tables 1 and 2. The antimicrobial properties of the compounds according to the minimum inhibitory concentration are as follows:

S. aureus: Na[**4**] > Na[**7**] > Thiam > Na[**8**] > Na_3[**5**]
S. pyogenes: Na[**4**] > Na[**7**] > Thiam > Na[**8**] > Na_3[**5**]
E. coli: Na[**4**] > Na[**7**] > Thiam > Na_3[**5**] > Na[**8**]
P. aeruginosa: Na[**4**] > Na_3[**5**] > Na[**7**] > Thiam > Na[**8**]
The antifungal effects against *Candida* spp.: Na[**7**] > Na[**4**] > Thiam > Na[**8**] > Na_3[**5**]

Nowadays more strains of pathogenic microorganisms, including *Staphylococci*, *Streptococci* and *Enterobacteria*, become resistant to many of the available antibiotics and chemotherapeutic agents, creating a serious problem in the treatment of infectious diseases [17b,29]. Antimicrobial resistance has produced alarming situation worldwide. There is a serious risk that a growing proportion of infections, especially in hospitals, will become effectively untreatable [30–32]. For that reason the trials to request for new antimicrobial means are very indispensable. Our investigations presented in this study showed that the tested cobaltabisdicarbollide compounds express promising antimicrobial properties *in vitro* – comparable or even better than those of the broad spectrum antibiotic thiamphenicol (positive control). The most active among the compounds examined were Na[**4**] and Na[**7**]. Particularly important from a practical point of view is the fact that meticillin-resistant strain of *S. aureus* (TSA MRSA) and the strains of *P. aeruginosa* were shown to be sensitive to the tested substances. Meticillin-resistant *S. aureus* (MRSA) bacteria are a common cause of hospital- and community-acquired infections, which are difficult to treat and are associated with significant morbidity and mortality. There is great interest in preventing the transmission of MRSA and decolonizing persons who harbor these bacteria [33]. *P. aeruginosa* (primarily a nosocomial organism that most commonly colonizes respiratory secretions and urine) resistance to antimicrobials is also an important therapeutic consideration [34]. Whereas it has reported that boron containing peptidomimetics [2c], sulfonamide boronic acids [2d] and brominated boron difluoride (BF_2) chelated tetraarylazadipyrromethene molecules are proved to exhibit antimicrobial properties [2e], in the available literature there are no data about antimicrobial activity of cobaltabisdicarbollides. In addition, it has to be mentioned also that of the various known antibacterial agent classes, amphiphilic compounds act through perturbation and disruption of the prokaryotic membrane [35]. Cobaltabisdicarbollide is considered a weakly coordinating anion [11c] that although lacking the amphiphilic topology behaves as an anionic surfactant [36]. There are many reports of linear polycationic agents but only a few descriptions of polyanionic antibacterial agents (e.g., sulfonated polystyrene) [37].

Table 3
Effect of cobaltabisdicarbollide complexes (CC_{50}, μg/ml) on viability and proliferation of cultured MDBK bovine kidney cells. CC_{50} was determined by thiazolyl blue tetrazolium bromide test (MTT) and neutral red uptake cytotoxicity assay (NR) after 72 h of treatment.

Compound	MTT	NR
Na[**7**]	15.3 ± 1.4	12.4 ± 2.1
Na[**3**]	25.7 ± 2.5	29.7 ± 1.9
Na[**4**]	37.4 ± 2.9	40.8 ± 3.1
Li[**8**]	>100	>100
Na_3[**5**]	>100	>100
Na[**6**]	19.4 ± 1.7	17.2 ± 0.8
H[**1**]	31.2 ± 3.7	26.8 ± 2.2
Thiamphenicol	>100	>100

The influence of the compounds tested on viability and proliferation of non-tumor mammalian cells was also evaluated. The investigations were performed by MTT test and NR cytotoxicity assay after 72 h of cell treatment. The effective concentrations (CC_{50}) at which the examined cobaltabisdicarbollides decreased by 50% the number of viable bovine kidney cells as compared to the non-treated controls are presented in Table 3. The results obtained revealed that among the cobaltabisdicarbollides investigated, compound [**7**]$^-$ expresses the highest cytotoxic activity while compounds [**5**]$^-$ and [**8**]$^-$ show the lowest cytotoxicity. Thus, the viability of MDBK cells cultured for 72 h in the presence of 50 μg/ml [**5**]$^-$ was calculated to be 102.8 ± 6.4%. In comparison, >98.5% of the treated bovine kidney cells was alive even after treatment with 200 μg/ml thiamphenicol.

In the light of interesting antimicrobial properties of the cobaltabisdicarbollides investigated, some more details have to be mentioned: 1) One of the most promising antibacterial agents Na[**4**], has also demonstrated to possess comparatively to the other cobaltabisdicarbollides moderate toxicity in cultured non-tumor cells; 2) Cobaltabisdicarbollide Na[**7**] was found to express the highest cytotoxic and antiproliferative as well as antimicrobial properties. It has to be remained that the biological activity of *cis*-platin – the world's leading anti-tumor drug for the modern chemotherapy of human cancer, was accidentally discovered in 1965 by Barnet Rosenberg and his coworkers who reported first the inhibitory activity of this compound on *E. coli* division [38,39]; 3) Cobaltabisdicarbollide Na_3[**5**] that is effective against *P. aeruginosa* is relatively low toxic for MDBK cells; 4) Cobaltabisdicarbollide H[**1**] was shown to express comparatively lower antibacterial and antifungal properties as compared to its derivatives.

At this stage, the mechanism of antimicrobial action of the compounds examined has not been elucidated. It seems, however, that the mechanism of action is not related to the synthesis of cell envelope, as Gram-positive and Gram-negative microorganisms exhibit sensitivity. In the literature available, there are few reports about antimicrobial activity of such compounds. It has recently been reported that ferrocene-substituted carborane derivative could act on bacteria via damaging the cell walls, destabilizing cell

Table 2
Minimum inhibitory concentration (MIC_{90}) of cobaltabisdicarbollide complexes on pathogenic microorganisms.

		MIC_{90}				
Microorganism	Number of strains	Na[**7**]	Li[**8**]	Na[**4**]	Na_3[**5**]	Thiam.
S. aureus	4	25.5 ± 9.2	72.0 ± 20.4	20.3 ± 4.0	88.0 ± 48.0	38.5 ± 10.7
S. pyogenes	4	6.3 ± 5.5*	52.0 ± 24.0	5.0 ± 2.4*	96.0 ± 36.9	34.0 ± 14.4
E. coli	4	14.4 ± 4.0	52.0 ± 24.0	8.0 ± 0.0*	43.5 ± 25.0	25.0 ± 10.4
P. aeruginosa	4	36.0 ± 20.0	43.5 ± 25.0	15.0 ± 12.0	34.0 ± 22.0	37.0 ± 10.1
Candida spp.	4	2.8 ± 0.8**	56.0 ± 16.0	4.5 ± 1.7**	64.0 ± 0.0***	28.5 ± 7.0

Significantly lower MICs versus wide-spectrum antibiotic thiamphenicol (used as positive control) are presented as follows: *$P < 0.05$, **$P < 0.01$, ***$P < 0.001$ vs. thiamphenicol.

membranes and inducing the leakage of cellular contents including nucleic acids and proteins [40]. This as well as other hypotheses can be explored in our future studies.

In summary, the cobaltabisdicarbollides examined in the present study demonstrate antimicrobial efficacy especially Na[**7**] and Na[**4**] and merit further investigations to clarify mechanism(s) of action and biological safety of these compounds. The knowledge concerning the relationship between the physical and chemical structure of such cobaltabisdicarbollides and their biological activities will facilitate the design of drugs with improved antimicrobial properties.

Acknowledgment

This work was supported by MEC (CTQ2010-16237), the Generalitat de Catalunya 2009/SGR/279, a bilateral project (2007 BG0017) between Institute of Experimental Pathology and Parasitology (Bulgarian Academy of Sciences) and Institute of Material Science (C.S.I.C.).

References

[1] (a) M. Scholz, E. Hey-Hawkins, Chem. Rev. 111 (2011) 7035;
(b) F. Issa, M. Kassiou, L.M. Rendina, Chem. Rev. 111 (2011) 5701;
(c) N.P.E. Barry, P.J. Sadler, Chem. Soc. Rev. 41 (2012) 3264;
(d) I.B. Sivaev, V.I. Bregadze, Eur. J. Inorg. Chem. (2009) 1433.
[2] (a) A.A. Alencar de Queroz, G.A. Abraham, M.A. Pires Camillo, O.Z. Higa, G.S. Silva, M.M. Fernandez, J. San Roman, J. Biomater. Sci. Polym. Ed. 17 (2006) 689;
(b) S.J. Baker, T. Akama, Y.K. Zhang, V. Sauro, C. Pandit, R. Singh, M. Kully, J. Khan, J. Plattner, S.J. Benkovic, V. Lee, K.R. Maples, Bioorg. Med. Chem. Lett. 16 (2006) 5963;
(c) A.S. Gorovoy, O.V. Gozhina, J.S. Svendsen, A.A. Domorad, G.V. Tetz, V.V. Tetz, T. Lejon, Chem. Biol. Drug Des. 81 (2013) 408;
(d) O. Eidam, C. Romagnoli, E. Caselli, K. Babaoglu, D.T. Pohlhaus, J. Karpiak, R. Bonnet, B.K. Shoichet, F. Prati, J. Med. Chem. 53 (2010) 7852;
(e) D.O. Frimannsson, M. Grossi, J. Murtagh, F. Paradisi, D.F. O'Shea, J. Med. Chem. 53 (2010) 7337.
[3] (a) A. Kalkanci, A.B. Güzel, Khalil II, M. Aydin, M. Ilkit, S. Kuştimur, Med. Mycol. 50 (2012) 585;
(b) J.W. Hicks, C.B. Kyle, C.M. Vogels, S.L. Wheaton, F.J. Baerlocher, A. Decken, S.A. Westcott, Chem. Biodiversity 5 (2008) 2415.
[4] Z. Sui, R. Salto, J. Li, C. Craik, P.R. Ortiz de Montellano, Bioorg. Med. Chem. 1 (1993) 415–422.
[5] X. Chen, K. Bastow, B. Goz, L. Kucera, S.L. Morris-Natschke, K.S. Ishag, Antivir. Chem. Chemother. 7 (1996) 108.
[6] A.D. Pivazyan, D.S. Matteson, L. Fabry-Asztalos, R.P. Singh, P.F. Lin, W. Blair, K. Guo, B. Robinson, W.H. Prusoff, Biochem. Pharmacol. 60 (2000) 927.
[7] P. Cigler, M. Kožíšek, P. Řezačova, J. Brynda, Z. Otwinowski, J. Pokorna, J. Plešek, B. Gruner, L. Dolečkova-Marešova, M. Maša, J. Sedlaček, J. Bodem, H. Kräusslich, V. Kral, Konvalinka, Proc. Natl. Acad. Sci. U. S. A. 102 (2005) 15394.
[8] R.N. Grimes, Carboranes, second ed., Academic Press, London, 2011.
[9] (a) J. Plešek, Chem. Rev. 92 (1992) 269;
(b) M.F. Hawthorne, A. Maderna, Chem. Rev. 99 (1999) 3421;
(c) B. Sivaev, V.I. Bregadze, Collect. Czech. Chem. Commun. 64 (1999) 783.
[10] M.F. Hawthorne, D.C. Young, T.D. Andrews, D.V. Howe, R.L. Pilling, A.D. Pitts, M. Reintjes, L.F. Warren Jr., P.A. Wegner, J. Am. Chem. Soc. 90 (1968) 879.
[11] (a) C. Viñas, S. Gomez, J. Bertran, F. Teixidor, J.F. Dozol, H. Rouquette, Chem. Commun. (1998) 191;
(b) C. Viñas, S. Gomez, J. Bertran, F. Teixidor, J.F. Dozol, H. Rouquette, Inorg. Chem. 37 (1998) 3640;
(c) B. Grüner, J. Plešek, J. Báča, I. Císařová, J.F. Dozol, H. Rouquette, C. Viñas, P. Selucký, J. Rais, New J. Chem. 26 (2002) 1519.
[12] (a) C. Masalles, S. Borrós, C. Viñas, F. Teixidor, Adv. Mater. 12 (2000) 1199;
(b) C. Masalles, J. Llop, C. Viñas, F. Teixidor, Adv. Mater. 14 (2002) 826;
(c) C. Masalles, S. Borrós, C. Viñas, F. Teixidor, Adv. Mater. 14 (2002) 449.
[13] (a) E. Hao, M.G.H. Vicente, Chem. Commun. (2005) 1306;
(b) V.I. Bregadze, I.B. Sivaev, S.A. Glazun, AntiCancer Agents Med. Chem. 6 (2006) 75;
(c) Z.J. Lesnikowski, E. Paradowska, A.B. Olejniczak, M. Studzinska, P. Seekamp, U. Schußler, D. Gabel, R.F. Schinazi, J. Plešek, Bioorg. Med. Chem. 13 (2005) 4168;
(d) B.A. Wojtczak, B. Gruner, Z.J. Lesnikowski, Chem. Eur. J. 14 (2008) 10675.
[14] (a) R.J. Paxton, B.G. Beatty, M.F. Hawthorne, A. Varadarajan, L. Williams, F.L. Curtis, C.B. Knobler, J.D. Beatty, J.E. Shively, Proc. Natl. Acad. Sci. U. S. A. 88 (1991) 3387;
(b) L. Guan, L.A. Wims, R.R. Kane, M. Smuckler, S.L. Morrison, M.F. Hawthorne, Proc. Natl. Acad. Sci. U. S. A. 95 (1998) 13206;
(c) R.A. Watson-Clark, M.L. Banquerigo, K. Shelly, M.F. Hawthorne, E.L. Brahn, Proc. Natl. Acad. Sci. U. S. A. 95 (1998) 2531;
(d) A. Nakanishi, L. Guan, R.R. Kane, H. Kasamatsu, M.F. Hawthorne, Proc. Natl. Acad. Sci. U. S. A. 96 (1999) 238.
[15] (a) S.R. Cherry, Phys. Med. Biol. 49 (2004) R13;
(b) O.O. Sogbein, P. Merdy, P. Morel, J.F. Valliant, Inorg. Chem. 43 (2004) 3032;
(c) A.E.C. Green, P.W. Causey, A.S. Louie, A.F. Armstrong, L.E. Harrington, J.F. Valliant, Inorg. Chem. 45 (2006) 5727;
(d) E.Z. Mohamed, N. Janzen, M. Blacker, J.F. Valliant, Chem. Eur. J. 18 (2012) 11071.
[16] V.I. Bregadze, S.A. Glazun, Russ. Chem. Bull. Int. Ed. 56 (2007) 643.
[17] (a) C. MacDougall, R.E. Polk, Clin. Microbiol. Rev. 18 (2005) 638;
(b) D.H. Lloyd, Vet. Dermatol. (2012) 299;
(c) T.-F. Mah, G.A. O'Toole, Trends Microbiol. 9 (2001) 34.
[18] (a) P. Farràs, F. Teixidor, R. Kivekäs, R. Sillanpää, C. Viñas, B. Grüner, I. Cisarova, Inorg. Chem. 47 (2008) 9497;
(b) V. Šícha, P. Farràs, B. Štíbr, F. Teixidor, B. Grüner, C. Viñas, J. Organomet. Chem. 694 (2009) 1599;
(c) P. Farràs, A. Cioran, V. Šícha, F. Teixidor, B. Štíbr, B. Grüner, C. Viñas, Inorg. Chem. 48 (2009) 8210.
[19] (a) F. Teixidor, J. Pedrajas, I. Rojo, C. Viñas, R. Kivekäs, R. Sillanpää, I. Sivaev, V. Bregadze, S. Sjöberg, Organometallics 22 (2003) 3414;
(b) J. Plesek, S. Hermánek, A. Franken, I. Cisarova, C. Nachtigal, Collect. Czech. Chem. Commun. 62 (1997) 47.
[20] I. Rojo, F. Teixidor, C. Viñas, R. Kivekäs, R. Sillanpää, Chem. Eur. J. 10 (2004) 5376.
[21] J. Rak, B. Dejlová, H. Lampová, R. Kaplánek, P. Matějíček, P. Cígler, V. Král, Mol. Pharmaceutics 10 (2013) 1751.
[22] A.W. Bauer, W.M. Kirby, J.C. Cherris, M. Truck, Am. J. Clin. Pathol. 45 (1966) 493.
[23] J.A. Andrews, J. Antimicrob. Chemother. 48 (Suppl. S1) (2001) 5.
[24] H.C. Davison, M.E.J. Woolhouse, J.C. Low, Trends Microbiol. 8 (2000) 554.
[25] H.M. Ericsson, J.S. Sherris, Acta Path. Microbiol. Scand. (Suppl. 217) (1971) 3.
[26] M.C. Rodríguez-Argüelles, E.C. López-Silva, J. Sanmartín, P. Pelagatti, F. Zani, J. Inorg. Biochem. 99 (2005) 2231.
[27] T. Mosmann, J. Immunol. Methods 65 (1983) 55.
[28] E. Borenfreund, J. Puerner, Toxicol. Lett. 24 (1985) 119.
[29] (a) D.R. Peaper, M.V. Kulkarni, A.N. Tichy, M. Jarvis, T.S. Murray, M.E. Hodsdon, Bioanalysis 5 (2013) 147;
(b) O. Megged, M. Assous, G. Weinberg, Y. Schlesinger, Isr. Med. Assoc. J. 15 (2013) 27.
[30] I. Stojiljkovic, V. Kumar, N. Srinivasan, Mol. Microbiol. 31/32 (1999) 429.
[31] J. Conly, Can. Med. Assoc. J. 167 (2002) 885.
[32] D.M. Livermore, Clin. Microbiol. Infect. 10 (2004) 1.
[33] (a) M.R. Hanson, C.L. Chung, J. Drugs Dermatol. 8 (2009) 281;
(b) K.W. McConeghy, D.J. Mikolich, K.L. LaPlante, Pharmacotherapy 29 (2009) 263.
[34] B.A. Cunha, Semin. Respir. Infect. 17 (2002) 231.
[35] S.P. Denyer, Int. Biodeterior. Biodegrad. 36 (1995) 227.
[36] (a) G. Chevrot, R. Schurhammer, G. Wipff, J. Phys. Chem. B 110 (2006) 9488;
(b) P. Matejicek, P. Cigler, K. Prochazka, Langmuir 22 (2006) 575;
(c) P. Bauduin, S. Prevost, P. Farras, F. Teixidor, O. Diat, T. Zemb, Angew. Chem. Int. Ed. 50 (23) (2011) 5298.
[37] (a) R.A. Anderson, K.A. Featherguill, X.H. Diao, M.P. Cooper, R. Kirkpatrick, B.C. Herold, G.F. Donzel, C.J. Chany, D.P. Waller, W.F. Rencher, L.J. Zaneveld, J. Androl. 23 (2002) 426;
(b) B.C. Herold, N. Bourne, D. Marcellino, R. Kirkpatrick, D.M. Strauss, L.J. Zaneveld, D.P. Waller, R.A. Anderson, C.J. Chany, B.J. Barham, L.R. Stanberry, M.D. Copper, J. Infect. Dis. 181 (2000) 770;
(c) S.R. Meyers, F.S. Juhn, A.P. Griset, N.R. Luman, M.W. Grinstaff, J. Am. Chem. Soc. 130 (2008) 14444.
[38] B. Rosenberg, L. Van Camp, T. Krigas, Nature 205 (1965) 698.
[39] B. Lippert, in: B. Lippert (Ed.), Cisplatin. Chemistry and Biochemistry of a Leading Anticancer Drug, Verlag Helvetica Chimica Acta, Zurich, 1999.
[40] S. Li, Z. Wang, Y. Wei, C. Wu, S. Gao, H. Jiang, X. Zhao, H. Yan, X. Wang, Biomaterials 34 (2013) 902.